RATCHET EFFECT IN MESOSCOPIC SYSTEMS

A THESIS SUBMITTED TO
THE GRADUATE SCHOOL OF NATURAL AND APPLIED SCIENCES
OF
THE MIDDLE EAST TECHNICAL UNIVERSITY

BY

UĞUR YİĞİT İNKAYA

IN PARTIAL FULFILLMENT OF THE REQUIREMENTS FOR THE DEGREE OF

MASTER OF SCIENCE

IN

THE DEPARTMENT OF PHYSICS

DECEMBER 2005

Approval of the Graduate School of Natural and Applied Sciences.

Prof. Dr. Canan Özgen
Director

I certify that this thesis satisfies all the requirements as a thesis for the degree of Master of Science.

Prof. Dr. Sinan Bilikmen
Head of Department

This is to certify that we have read this thesis and that in our opinion it is fully adequate, in scope and quality, as a thesis for the degree of Master of Science.

Assist. Prof Dr. Sadi Turgut
Supervisor

Examining Committee Members

Prof. Dr. Şinasi Ellialtıoğlu (METU, Phys) _____

Assist. Prof. Dr. Sadi Turgut (METU, Phys) _____

Prof. Dr. T. Aliev (METU, Phys) _____

Prof. Dr. Ramazan Sever (METU, Phys) _____

Assoc. Prof. Dr. Oğuz Gülseren(Bilkent University) _____

"I hereby declare that all information in this document has been obtained and presented in accordance with academic rules and ethical conduct. I also declare that, as required by these rules and conduct, I have fully cited and referenced all material and results that are not original to this work."

Name Surname : UĞUR YİĞİT İNKAYA

Signature :

ABSTRACT

RATCHET EFFECT IN MESOSCOPIC SYSTEMS

İNKAYA, UĞUR YİĞİT

M.S., Department of Physics

Supervisor: Assist. Prof Dr. Sadi Turgut

DECEMBER 2005, 51 pages

Rectification phenomena in two specific mesoscopic systems are reviewed. The phenomenon is called ratchet effect, and such systems are called ratchets. In this thesis, particularly a rocked quantum-dot ratchet, and a tunneling ratchet are considered. The origin of the name is explained in a brief historical background. Due to rectification, there is a net non-vanishing electronic current, whose direction can be reversed by changing rocking amplitude, the Fermi energy, or applying magnetic field to the devices (for the rocked ratchet), and tuning the temperature (for the tunneling ratchet). In the last part, a theoretical examination based on the Landauer-Büttiker formalism of mesoscopic quantum transport is presented.

Keywords: Ratchets, Brownian motors, Rectification, Quantum transport, Mesoscopics, Non-equilibrium process, Brownian motion.

ÖZ

MEZOSKOPİK SİSTEMLERDE ÇARK ETKİSİ

İNKAYA, UĞUR YİĞİT

Yüksek Lisans, Fizik Bölümü

Tez Yöneticisi: Yrd. Doç. Dr. Sadi Turgut

ARALIK 2005, 51 sayfa

İki spesifik mezoskopik sistemde görülen rektifikasyon fenomeniyle ilgili mevcut literatür tarandı ve analiz edildi. Bu fenomene çark etkisi, bu tip sistemlere de çarklar denmektedir. Bu tezde, özellikle sarsılan kuvantum nokta çarkları ve tünelleme çarkları incelenmiştir. Bu sistemlerin ve fenomenin isimsel kökeni kısa bir tarihçeyle açıklanmıştır. Rektifikasyondan dolayı, sarsma genliği veya Fermi enerjisini değiştirerek, veya cihazlara manyetik alan uygulayarak (sarsılan çarklar için), veya sıcaklığı ayarlayarak (tünelleme çarkları için) yönü tersine çevrilebilen, net olarak kaybolmayan bir elektronik akım görülebilir. Son kısımda, mezoskopik kuvantum transportun Landauer-Büttiker formalizmi bazlı bir teorik inceleme sunulmuştur.

Anahtar Kelimeler: Rektifikasyon, Kuvantum transport, Mezoskopik fizik, Dengedışı süreçler, Brown hareketi.

To my family

ACKNOWLEDGMENTS

I would like to thank to Dr. Sadi Turgut for his support and supervision in this work.

TABLE OF CONTENTS

LIST OF FIGURES

FIGURES

CHAPTER 1

INTRODUCTION

1.1 Introduction

The concept of ratchet can be traced back to a conference talk by Smoluchowski in Münster 1912 [3]. The main problem is about the possibility of extracting useful work out of unbiased random fluctuations. In the case of macroscopic fluctuations, one can easily give several examples of mechanical and electrical rectifiers such as the wind-mill, the self-winding wristwatch etc. However, ratchets require microscopic fluctuations, which is more subtle. The following gedankenexperiment, which is of fundamental importance concerning the conceptual development, was firstly presented by Smoluchowski and later popularized and extended by Feynman [4].

The main ingredient of Smoluchowski and Feynman's gedankenexperiment is an axle with at one end paddles and at the other end a so-called ratchet, reminiscent of a circular saw with asymmetric saw-teeth. The whole device is surrounded by a gas at thermal equilibrium. So, if it could freely turn around, it would perform a rotatory Brownian motion due to random impacts of gas molecules on the paddles. The idea is to rectify this unbiased random motion with the help of a pawl (Fig 1.1). It is indeed quite suggestive that the pawl will admit the saw-teeth to proceed without much effort into one direction (henceforth called "forward") but practically exclude a rotation in the opposite ("backward") direction. In other words, it seems quite convincing that the whole gadget will perform on the average a systematic rotation in one direction, and this would in fact be so even if a small load in the opposite

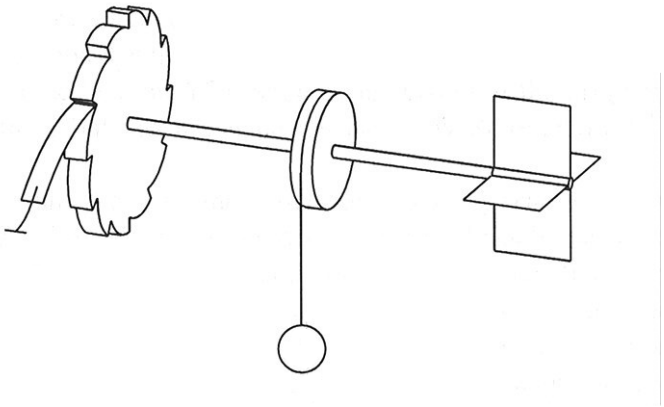

Figure 1.1: Ratchet and pawl (From [3])

direction is applied.

Astonishingly enough, the naive expectation is wrong: In spite of the built-in asymmetry, no preferential direction of motion is possible. Otherwise, such a gadget would represent a perpetuum mobile of the second kind, in contradiction to the second law of thermodynamics. The culprit must be our assumption about the working of the pawl. Since the impacts of the gas molecules take place on a microscopic scale, the pawl needs to be extremely small and soft in order to admit a rotation even in the forward direction. As Smoluchowski points out, the pawl itself is therefore also subjected to non-negligible random thermal fluctuations. So, every once in a while the pawl lifts itself up and the saw-teeth can freely travel underneath. Such an event clearly favors on the average a rotation in the "backward" direction (if there is a load). At overall thermal equilibrium (the gas surrounding the paddles and the pawl being at the same temperature) the detailed quantitative analysis indeed results in the subtle probabilistic balance which just rules out the functioning of such a perpetuum mobile. Note that the preceding discussion does not require any quantum concept.

It is possible to determine whether a given system is physically equivalent to the ratchet-and-pawl gadget. To accomplish this task, one must find out what fundamental physical principles the ratchet-and-pawl device is based on. It can easily be seen that the system has two important basic parts: A heat bath, or a thermal reservoir (the gas surrounding the gadget); and an asymmetric potential (for example, see

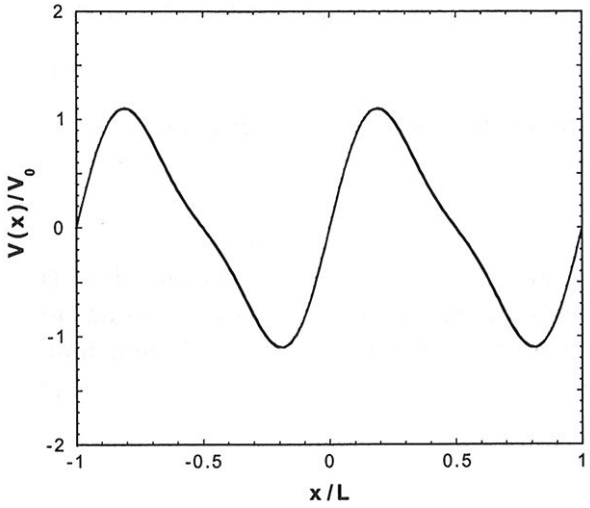

Figure 1.2: Typical example of a ratchet-potential V, where $V(x) = V_0[\sin(2\pi x/L) + 0.25\sin(4\pi x/L)]$, periodic in space with period L and with broken spatial symmetry. Plotted in dimensionless units (From [3]).

Fig. 1.2) (the ratchet co-operating with the pawl). Firstly, thermal reservoir is the source of unbiased random fluctuations, which causes a Brownian motion (e.g. of paddles) in the system. Secondly, however idealized the system is, there must be a spring in the pawl. The pawl must return back after coming off a tooth, so the spring is necessary. Thus, the system gains a potential via this spring. Since the ratchet has asymmetric saw-teeth to move under the pawl, this potential is asymmetric. As a result, any equivalent system must have the features listed above. Henceforth, ratchet-and-pawl system will simply be called ratchet, which is also the name of any equivalent system.

Before starting to search for possibilities of rectification in ratchets, consider the following system, consisting of a particle, having one degree of freedom, a one dimensional asymmetric periodic potential (Fig. 1.2) that the particle is subjected to, and a heat bath with which the particle interacts. In other words, there is a Brownian particle, which is a particle performing Brownian motion, moving in one dimensional space and having a periodic potential with broken spatial symmetry. Clearly this system is a ratchet, and it introduces a transport problem as well. So the ratchet and pawl problem can be considered as a transport problem. Impossibility of obtaining a directed rotation in Smoluchowski-Feynman ratchet corresponds to the impossibility of obtaining a directed transport in the system described above. Classically, it can be

shown by using a simple stochastic model that the associated probability density of the particle goes to the Boltzmann distribution and the corresponding average particle current vanishes in the long-time limit $t \to \infty$, as if there were not an asymmetric potential [3]. In other words, asymptotically there is again a probabilistic balance between the motions in different directions, which implies that the average displacement of the particle is zero, i.e. it goes nowhere on the average and thus there is no directed transport. By the so-called long-time asymptotic behavior, we mean the steady-state motion of the particle, similar to the motion of Smoluchowski-Feynman ratchet when it is initially at rest, namely a Brownian movement. Thus, the model verifies that it is impossible to rectify the motion of a ratchet in equilibrium conditions as required by the second law thermodynamics. Hence, ratchets have to be driven away from thermal equilibrium by an additional deterministic or stochastic perturbations to obtain a rectification. For instance, one can show that the addition of an alternating driving force to the system gives rise to a non-vanishing particle current, or a rectification [3]. Such a system is called a rocking ratchet.

Hitherto only classical ratchets were taken into account. Classical ratchets are the ratchets that operate according to the principles of classical mechanics. Then the idea of quantum ratchets is naturally conceivable. Consider the ratchet introduced in the previous paragraph. Suppose that the particle has also quantum behavior. Consequently, it suffers reflections during its motion in the potential field, interference effects arises, and also the particle may tunnel through classically forbidden regions. This may be considered as a qualitative example of a so-called quantum ratchet. This thesis contains two concrete examples of such devices.

The two examples are a quantum-dot ratchet and a tunneling ratchet, which are both made out of quantum dots [2]. The quantum-dot ratchet was realized by using a triangular quantum dot, which is a triangular electron cavity (Fig. 1.3a). This cavity is manufactured using a GaAs/AlGaAs heterostructure. The experimental system is a so-called "mesoscopic" semiconductor device, where electron transport effects can be studied in a regime that lies between "large", macroscopic systems, in which classical, ohmic behavior is observed, and extremely small, fully quantum-mechanical systems, such as atoms. At the interface of a GaAs/AlGaAs heterostructure, a sheet of electrons, which forms a so-called two dimensional electron gas (2DEG in short),

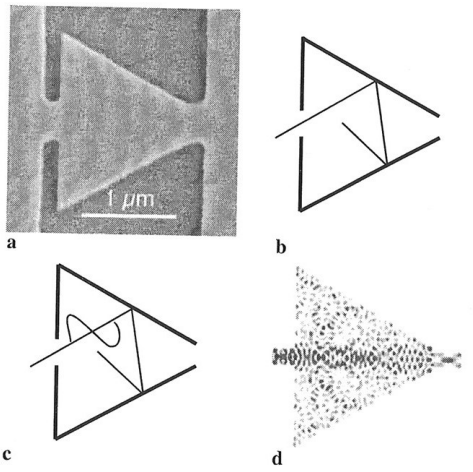

Figure 1.3: (a) Scanning electron micrograph of a triangular electron cavity (top view). (b) At low temperatures electrons move along straight trajectories between collisions with the boundaries. (c) When electron transport is phase coherent, a semi-classical description of transport is useful. (d) A fully quantum mechanical description (From [5]).

is located. In Fig. 1.3a, there is a top-view scanning electron micrograph of the electron cavity. The darker areas in the image are trenches patterned by electron beam lithography and subsequent wet-etching. The etched trenches electrically isolate the inner part of the triangle -the electron cavity- from the surrounding 2DEG areas, except for two narrow openings (so-called point contacts), visible at the tip and in the center of the base of the triangle. Quantum-dot ratchets utilize the sensitive response of electron-wave interference to an external electric field to partially rectify an ac voltage, which is a distinct mechanism from that in a tunneling ratchet, where rectification is due to the non-linear response of a tunneling barrier. In this device, it is possible to reverse the net ratchet current by tuning the temperature.

1.2 Outline and scope

In this chapter, we put emphasis on the introduction of some essential terms,main ideas and give brief information on the content of remaining chapters.

The purpose of Chapter 2 is to present basic concepts and formulae related to quantum ratchets. Section 2.1 gives necessary information about 2DEG. In section 2.3 and 2.4 the equation of motion for the electrons moving in a 2DEG is discussed.

Section 2.3 contains brief information about the characteristic lengths of motion of electrons in conductors.

Chapter 3 is devoted to a review of the experiments involving quantum-dot ratchets and tunneling ratchets, contained in sections 3.2 and 3.3, respectively.

Chapter 4 gives theoretical examinations and interpretations of the experimental results. Section 4.1 and 4.2 presents theoretical explanations based on a model applied previously. Section 4.3 is about our model and corresponding solution procedure.

Chapter 5 gives a conclusion.

CHAPTER 2

FUNDAMENTAL CONCEPTS AND FORMULAE

Typical dimension of the cavity shown in Fig. 1.3 is of the order of a micrometer, which is much smaller than the characteristic length scales for electron scattering at low temperatures ($T < 10$ K). Under these physical conditions, electrons begin to move in such a way that the motion can be well-described by a single-particle picture, in which electron trajectories between boundary collisions are rectilinear. This limiting behavior of electrons is called the ballistic limit. In analogy with the game of billiards, ballistic two-dimensional cavities are often referred to as electron billiard.

There are three length scales relevant to the observation of quantum effects in electron billiards: [2] (a) the phase coherence length, ℓ_ϕ; (b) the electron wavelength at the Fermi energy, λ_{F}; (c) and the characteristic length for tunneling effects. Phase coherence length is the length scale over which the so-called phase memory, i.e. wave behavior, of electrons persists. So this scale is of great importance for the observation of electronic wave-interference effects. While phase coherence is preserved in elastic scattering processes, particularly the collisions between electrons and the billiard walls, ℓ_ϕ depends on inelastic scattering events, such as electron-electron or electron-phonon interactions where through a transfer of energy, the electron leaves an imprint in the environment. This makes ℓ_ϕ a temperature-dependent quantity, which can exceed tens of micrometers at sub-Kelvin temperatures. However, it decreases quickly with increasing temperature and is typically less than a micrometer at about 5 K. This property makes it possible to switch on and off wave-interference

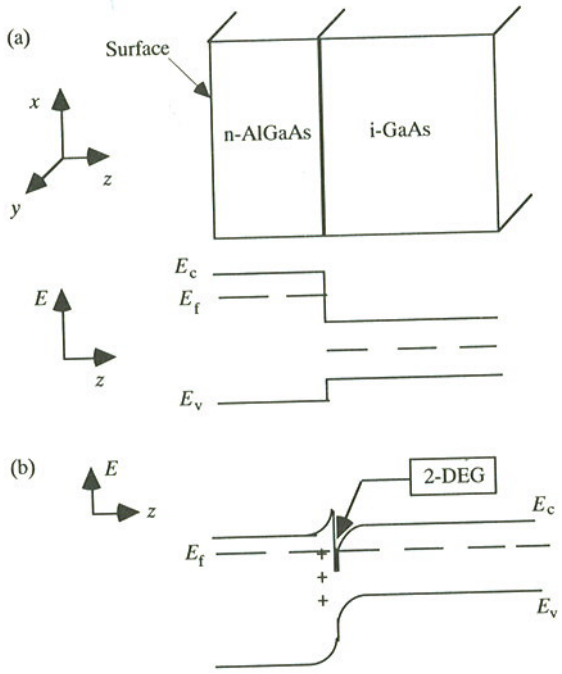

Figure 2.1: Conduction valence band line-up at a junction between an n-type AlGaAs and intrinsic GaAs (From [1]), (a) before and (b) after charge transfer has taken place. Note that this is a cross-sectional view. Patterning (as shown in Fig.3a) is done on the surface ($x - y$ plane) using lithographic techniques.

effects experimentally by tuning the temperature around 1 K – a very useful tool. As another quantum mechanical feature, the observation of effects relevant to energy quantization due to spatial confinement is critically influenced by the electron wavelength. For example, quantization effects are observable in the conductance of the point contacts of the cavity shown in Fig. 1.3a if λ_{F} is of the order of contact width.

2.1 Two-dimensional electron gas

Recent work on mesoscopic conductors has largely been based upon GaAs-AlGaAs heterojunctions in which a thin conducting layer is formed at the interface between undoped intrinsic GaAs (shortly i-GaAs) and n-type impurity doped AlGaAs (shortly n-AlGaAs) [1]. To understand the process that forms this conducting layer, one should consider the results of bringing the two material layers, namely GaAs and AlGaAs layers, in contact. Before the contact, each material is in its own equilibrium state with definite values of the Fermi energy. But, immediately after the contact,

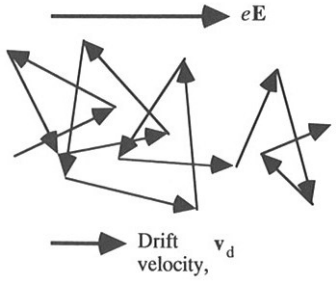

Figure 2.2: In the presence of an electric field the electrons acquire a drift velocity superposed on their random motion (From [1]).

resultant system consisting of the two layers, does not have a definite Fermi energy, thus non-equilibrium conditions arise (Fig. 2.1(a)). The Fermi energy (shown by E_{f}) in the wide-gap n-AlGaAs layer is higher than that in the narrow-gap GaAs layer due mainly to the presence of donor impurities. Accordingly electrons diffuse from the n-AlGaAs through i-GaAs, leaving behind positively charged donors until a new equilibrium is established. This space charge gives rise to an electrostatic potential that causes the bands to bend as shown in Fig. 2.1(b). At equilibrium the Fermi energy is constant everywhere. The electron density is sharply peaked near the GaAs-AlGaAs interface (where the Fermi energy is inside the conduction band) forming a thin conducting layer which is usually referred to as the two-dimensional electron gas (2DEG).

The carrier concentration in a 2DEG typically ranges from $2 \times 10^{11}/\mathrm{cm}^2$ to $2 \times 10^{12}/\mathrm{cm}^2$ and can be depleted by applying a negative voltage to a metallic gate deposited on the surface. What makes the 2DEG in GaAs important is its high mobility due to the extremely low scattering rates that have been achieved [1].

2.1.1 Mobility

In equilibrium the conduction electrons perform Brownian motion, i.e. they move around randomly without resulting any net displacement on average. However, an applied electric field $\mathbf{E}$ affects the motion in such a way that the electrons acquire a so-called drift velocity $\mathbf{v}_d$ after some time elapsed (Fig. 2.2). This time is a characteristic quantity and it is called the momentum relaxation time, denoted by τ_{m} [1]. When the electrons have a constant nonzero average velocity, the system reaches a steady

state, where the rate at which the electrons receive momentum from the applied field is exactly equal to the rate at which they lose momentum ($\mathbf{p}$) because of scattering forces. Accordingly,

$$\dot{\mathbf{p}}_{\text{scattering}} = \dot{\mathbf{p}}_{\text{field}} \tag{2.1}$$

Hence,

$$\frac{m\mathbf{v}_d}{\tau_{\text{m}}} = e\mathbf{E} \Rightarrow \mathbf{v}_d = \frac{e\tau_{\text{m}}}{m}\mathbf{E} \tag{2.2}$$

where the coefficient of proportionality between $\mathbf{v}_d$ and $\mathbf{E}$ is called mobility. Mobility is a temperature-dependent quantity: It increases with decreasing temperature due to the increase in momentum relaxation time. In GaAs-AlGaAs heterojunctions, the donor impurities of AlGaAs is usually doped away from the interface to increase the mobility of electrons in 2DEG. In this way, carrier concentrations of $10^{12}/\text{cm}^2$ in a layer of thickness $\sim 100\mathring{A}$ (equivalent bulk concentration of $10^{18}/\text{cm}^3$) have been obtained with mobilities in excess of $10^6\text{cm}^2/V\cdot s$, which is much larger than that of bulk semiconductors. In bulk semiconductors, with a donor concentration of $10^{17}/\text{cm}^3$ the highest mobility is less than $10^4\text{cm}^2/\text{Vs}$. Higher mobilities can be obtained with un-doped samples but this is not very useful since there are only a few conduction electrons.

2.2 Single-band effective-mass equation

Although electronic conduction in semiconductors can occur either through electrons in the conduction band or through holes in the valence band, most experiments on mesoscopic conductors involve the flow of electrons in the conduction band and it will be assumed that this is the case for our systems.

The electrons in a perfect crystal can be described by the Bloch wavefunctions

$$\Psi(\mathbf{r}) = u_{\mathbf{k}}(\mathbf{r})e^{i\mathbf{k}\cdot\mathbf{r}} \quad , \tag{2.3}$$

where $u_{\mathbf{k}}(\mathbf{r})$ is a periodic function with the periodicity of the lattice, depending on the band used, and $\mathbf{k}$ is the wavevector in the first Brillouin zone. When an external potential or an external magnetic field is applied to the crystal, the Schrödinger equation has to be solved again to compute the new eigenfunctions. When the external potential and magnetic field are varying slowly compared to interatomic distances and

the field is not too strong, then the interband coupling can be ignored and the Bloch wavefunctions in Eq. (2.3) for the lowest conduction band can be used to construct good approximate wavefunctions. In that case, one basically constructs wavepackets from the Bloch wavefunctions with the uncertainty Δk in the wavevector being small compared to Brillouin zone dimensions (the spread of the wavepacket is large compared to interatomic distances). If the band minimum is at Γ point, then for all practical purposes, one needs to look at wavepackets formed around $\mathbf{k} = 0$ value. In that case, it is possible to write the approximate wavefunction of the electrons as

$$\Psi(\mathbf{r}) = u_{\mathbf{k}=0}(\mathbf{r})\psi(\mathbf{r}) \quad , \tag{2.4}$$

where $\psi(\mathbf{r})$, which is called the envelope wavefunction, replaces the plane wave factor in the Bloch form in Eq. (2.3), obviously due to the loss of translational symmetry.

To obtain an effective Hamiltonian for the envelope wavefunction, we can insert Eq. (2.4) into the true Schrödinger equation of the crystal with the external potentials and fields added. In that case, it can be shown that the effective Hamiltonian, describing the behavior of the envelope, $\psi(\mathbf{r})$, is given as

$$[E_{\mathrm{c}} + \frac{(\mathrm{i}\hbar\nabla + e\mathbf{A})^2}{2m^*} + U(\mathbf{r})]\psi(\mathbf{r}) = E\psi(\mathbf{r}) \quad , \tag{2.5}$$

where $U(\mathbf{r})$ is the potential energy due to space-charge etc. and $\mathbf{A}$ is the vector potential [1]. Here E_{c} is the conduction-band minimum and m^* is the effective mass, defined through the dispersion relation for the energy eigenvalue of the Bloch wavefunction (2.3)

$$E(\mathbf{k}) \approx E_{\mathrm{c}} + \frac{\hbar^2}{2m^*}\mathbf{k}^2 \quad , \tag{2.6}$$

where higher order terms in the expansion are ignored and the effective mass is assumed to be isotropic (which is the case in the cubic crystal structures we are interested in).

It should be noted that in Eq. (2.5), the atoms of the crystal is not seen, their effect is included only through the modification of the mass to the effective mass and addition of conductance band minimum to the energy. Also, the envelope wavefunction $\psi(\mathbf{r})$ does not contain the rapid variation of the true wavefunction in atomic dimensions, the latter being taken care of by the factor $u_{\mathbf{k}=0}(\mathbf{r})$ which has nicely dropped out from the effective Schrödinger equation. The new effective equation (2.5), which

is called single-band effective mass equation, greatly simplifies the analysis of the complicated structures that can be constructed.

When there is a junction between two different crystals (such as the AlGaAs-GaAs heterojunctions), all we need to do is to let the band minimum E_{c} to be position dependent (in other words, E_{c} is included on an equal footing with the external potential $U(\mathbf{r})$). Also, the effective mass has to be position dependent, but in that case the effective Hamiltonian has to be carefully constructed for obtaining a correct hermitian operator.

2.2.1 Sub-bands

Consider the 2DEG depicted in Fig. 2.1(b). The electrons are able to propagate freely in the x-y plane but confined by some potential $U(z)$ in the $z-\mathrm{direction}$. Then the corresponding electronic wave functions (with $\mathbf{A}=0$, assuming zero magnetic field) can be written in the form

$$\psi(x,y,z) = \phi_n(z)\exp(\mathrm{i}k_x x)\exp(\mathrm{i}k_y y) \tag{2.7}$$

with the dispersion relation:

$$E = E_{\mathrm{c}} + \varepsilon_n + \frac{\hbar^2}{2m^*}(k_x^2 + k_y^2) \tag{2.8}$$

The index n numbers the different sub-bands each having a different wave function ϕ_n in the z-direction with energy eigenvalue ε_n [1]. Usually at low temperatures with low carrier densities only the lowest sub-band with $n=1$ is occupied and the higher sub-bands do not play any significant role. We can then ignore the z-dimension entirely and simply treat the conductor as a two-dimensional system in the x-y plane. Consequently, instead of Eq. (2.5) we can use the following equation:

$$[E_{\mathrm{s}} + \frac{(\mathrm{i}\hbar\nabla + e\mathbf{A})^2}{2m^*} + U(x,y)]\psi_{\mathrm{2D}}(x,y) = E\psi_{\mathrm{2D}}(x,y) \tag{2.9}$$

where $E_{\mathrm{s}} = E_{\mathrm{c}} + \varepsilon_1$. Here, ψ_{2D} is another envelope wavefunction defined through $\psi(x,y,z) = \phi_1(z)\psi_{\mathrm{2D}}(x,y)$. This simplification will generally be adopted throughout the thesis during the theoretical discussions.

When there is no magnetic field, the eigenfunctions for a free electron gas are obtained from Eq. (2.9) by setting $U=0$ and $\mathbf{A}=0$. The eigenfunctions have the

form

$$\psi_{\mathrm{2D}}(x,y) = \exp(\mathrm{i}k_x x)\exp(\mathrm{i}k_y y) \quad , \tag{2.10}$$

with eigenenergies

$$E = E_{\mathrm{s}} + \frac{\hbar^2}{2m^*}(k_x^2 + k_y^2) \quad . \tag{2.11}$$

2.3 Transverse modes (or magneto-electric sub-bands)

By depositing metallic gates on top of AlGaAs-GaAs heterojunctions, it is possible to deplete certain regions of the 2DEG from electrons in a controlled way. Also, by chemical etching, it is possible to physically remove certain parts of the AlGaAs-GaAs interface. With these methods, it is possible to confine the electrons further and construct numerous mesoscopic structures where quantum effects can be studied (one-dimensional quantum wires, zero-dimensional quantum dots etc.).

In here we will be interested only in confinement in one more direction (along y axis), where the electrons can flow in the other direction (along x axis). Both sides of the structure obtained is connected to 2DEG and by applying a potential difference between these and monitoring the current flow through the structure, quantum transport phenomena can be studied. First, we are going to investigate the case where the confinement is uniform, i.e., the external potential $U(x,y)$ in Eq. (2.9) depends only on y. Also we will assume that there is no magnetic field. In that case, the Schrödinger equation is separable and the particle is essentially free along x direction. Therefore, we can express the eigenfunctions of the Hamiltonian as $\psi_{\mathrm{2D}}(x,y) = \chi_n(y)e^{ikx}$ where the transverse wavefunctions χ_n satisfy

$$\left[\frac{p_y^2}{2m^*} + U(y)\right]\chi_n(y) = \epsilon_n\chi_n(y) \quad , \tag{2.12}$$

and the energy eigenvalue of the electron is

$$E = E_{\mathrm{s}} + \frac{\hbar^2 k^2}{2m^*} + \epsilon_n \quad . \tag{2.13}$$

As a result, several one-dimensional subbands form as a result of the confinement. The corresponding dispersion relations are depicted in Fig. 2.3.

Depending on the "width" of the wire (which is basically determined by the confinement potential $U(y)$), only a few or several of these subbands can be populated.

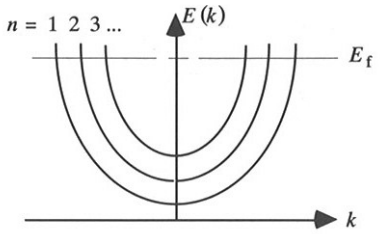

Figure 2.3: Dispersion relation, $E(k)$ vs. k for electric sub-bands arising from electrostatic confinement in zero magnetic field. Different sub-bands are indexed by n (From [1]).

Also, when the confinement is created by top gates, it is possible to move the subband minima above or below the Fermi energy, and hence change the number of populated subbands, by merely changing the gate voltage. As a result of this, several interesting experiments can be carried out on these structures. In analogy with the transverse modes ($\mathrm{TE}_{10}, \mathrm{TM}_{11}$ etc.) of electromagnetic wave-guides, such conductors are often called electron wave-guides.

The uniform confinement assumption above is not suitable for real structures since for a lot of cases, the width of the wire varies along the wire, in other words the confinement potential U depends on x as well. This may be by intention, for example a quantum dot is deliberately inserted somewhere into the wire, or by necessity such as in the "contacts", the regions where the wire is connected to 2DEG, or by unwanted irregularities (impurity atoms, irregular gates etc.). The general treatment of these non-uniformities is complicated and requires the solution of two-dimensional Schrödinger equation. However, when the non-uniformity is slowly varying, a scheme called adiabatic approximation works quite well.

We are going to assume that $U(x, y)$, the confinement potential, depends weakly on the x coordinate, i.e., it changes very slowly compared to the Fermi wavelength. We can still insist on solving the y-component of the Schrödinger equation separately. In that case we have the equation (2.12) transformed into

$$\left[\frac{p_y^2}{2m^*} + U(x, y)\right] \chi_n(y; x) = \epsilon_n(x)\chi_n(y; x) \quad , \tag{2.14}$$

where the coordinate x enters only as a parameter. In other words, we have a one-dimensional Hamiltonian which depends on a parameter x and we are solving the

eigenvalue equation for such an operator. Obviously, both the eigenfunctions $\chi_n(y;x)$ and the eigenenergies $\epsilon_n(x)$ will depend on the parameter. The eigenfunctions obtained will necessarily form a complete orthonormal basis, i.e.,

$$\int \chi_n(y;x)^* \chi_m(y;x) dy = \delta_{n,m} \quad , \tag{2.15}$$

$$\sum_n \chi_n(y_1;x)^* \chi_n(y_2;x) = \delta(y_1 - y_2) \quad . \tag{2.16}$$

For that reason, it is possible to expand any function of y in this basis for any value of x. For example, if the function is $f(y)$, then

$$f(y) = \sum_n a_n(x) \chi_n(y;x) \quad , \tag{2.17}$$

where

$$a_n(x) = \int \chi_n(y;x)^* f(y) dy \quad . \tag{2.18}$$

The expansion coefficients a_n should obviously depend on x.

At this stage, we expand the wavefunction $\psi_{2\mathrm{D}}(x,y)$ considered as a function of y in the orthonormal basis discussed above as

$$\psi_{2\mathrm{D}}(x,y) = \sum_n \phi_n(x) \chi_n(y;x) \quad , \tag{2.19}$$

where the expansion coefficients are now called $\phi_n(x)$. We then insert this expansion into the Schrödinger equation (2.9),

$$\sum_n -\frac{\hbar^2}{2m^*} \left(\phi_n'' \chi_n + 2\phi_n' \frac{\partial \chi_n}{\partial x} + \phi_n \frac{\partial^2 \chi_n}{\partial x^2} \right) + \epsilon_n \phi_n \chi_n = E \sum_n \phi_n \chi_n \quad . \tag{2.20}$$

We then multiply this equation by $\chi_m(y;x)^*$ and integrate along y. By carrying out the necessary simplifications we obtain

$$-\frac{\hbar^2}{2m^*} \left(\phi_m'' - 2i \sum_n K_{mn} \phi_n' - \sum_n (iK_{mn}' + (K^2)_{mn}) \phi_n \right) + \epsilon_m \phi_m = E \phi_m \quad , \tag{2.21}$$

where

$$K_{mn} = K_{mn}(x) = i \langle \chi_m \mid \partial_x \chi_n \rangle = i \int \chi_m(y;x)^* \frac{\partial \chi_n(y;x)}{\partial x} dy \quad , \tag{2.22}$$

are matrix elements of a hermitian matrix. Mathematically, solution of Eq. (2.21) is equivalent to the solution of Eq. (2.9), nothing is lost at this point. At this stage, we use the assumption that $U(x,y)$ is slowly varying with x. In that case, $\chi_n(y;x)$ is also slowly varying with x and therefore the matrix elements of K are small. Therefore,

we can drop all terms containing K in Eq. (2.21) and find the following "effective Hamiltonian" along conduction direction x,

$$\left(-\frac{\hbar^2}{2m^*}\frac{\partial^2}{\partial x^2}+\epsilon_m(x)\right)\phi_m(x)=E\phi_m(x) \quad . \tag{2.23}$$

In other words, the transverse eigenenergies $\epsilon_m(x)$ have become "effective potentials" along the conduction direction. The approximation we have made essentially tells us that there is no inter-sub-band transitions as the electrons move along the conduction direction. This assumption is justified as long as the confinement potential is slowly varying. If there is a sharp variation in the confinement potential (such as a suddenly changing width), then the electron makes transitions to various subbands and the approximation we have described above become useless.

One typically used confinement potential is the hard-wall potential where $U(x,y)=0$ when $|y|<W(x)/2$ and infinite otherwise. In that case, $W(x)$ is the exact width of the wire at the coordinate x. The transverse energy eigenvalues are

$$\epsilon_n(x)=\frac{\hbar^2\pi^2n^2}{2m^*W(x)^2} \quad . \tag{2.24}$$

In the adiabatic case, the electrons will see the narrowest parts of the wire as a potential barrier.

2.4 Characteristic lengths

A conductor usually shows ohmic behavior if its dimensions are much larger than certain characteristic lengths, namely, (1) the Fermi wavelength, (2) the mean free path, and (3) the phase-relaxation length. In addition to these, the screening length can also play a significant role particularly in low-dimensional conductors [1].

Wavelength (λ_{F}): At low temperatures the current is carried mainly by electrons having an energy close to the Fermi energy so that the Fermi wavelength is the relevant length. If the size of the conductor is comparable to Fermi wavelength, which is denoted by λ_{F}, then interference effects become important. In that case, exact places of impurities and walls are important for the determination of conductance. This leads to a nonlocal dependence of the current densities to applied electric fields which is a typical non-ohmic behavior.

Mean free path (L_{m}): An electron in a perfect crystal moves as if it were in vacuum but with a different mass. Any imperfection due to the presence of some factors, which are mainly related to crystal structure and dynamics, such as impurities, lattice vibrations (phonons) or other electrons leads to the scattering of the electron from one momentum state to another. The momentum relaxation time can be expressed in terms of the collision time by a relation of the form

$$\frac{1}{\tau_{\mathrm{m}}} \rightarrow \alpha_{\mathrm{m}} \frac{1}{\tau_{\mathrm{c}}} \tag{2.25}$$

where the factor α_{m} (lying between 0 and 1) denotes the "effectiveness" of an individual collision in destroying momentum.

The mean free path, L_{m}, is the distance that an electron travels before its initial momentum is destroyed; that is,

$$L_{\mathrm{m}} = \nu_{\mathrm{F}} \tau_{\mathrm{m}} \tag{2.26}$$

where ν_{F} is the Fermi velocity.

Phase-relaxation length (L_{φ}): Before explaining the meaning of the phase-relaxation length, let us discuss another quantity, the phase relaxation time (τ_{φ}), which is related to the former. In analogy with the momentum relaxation time one could write

$$\frac{1}{\tau_{\varphi}} \rightarrow \alpha_{\varphi} \frac{1}{\tau_{\mathrm{c}}} \tag{2.27}$$

where the factor α_{φ} denotes the effectiveness of an individual collision in destroying phase, which is a little more subtle process than the destruction of momentum. A more careful analysis is needed to define what the effectiveness factor α_{φ} is for different types of scattering processes.

As mentioned above, a relation between the two quantities that are denoted by L_{φ} and τ_{φ}, could be established. The obvious approach is to multiply by the Fermi velocity:

$$L_{\varphi} = \nu_{\mathrm{F}} \tau_{\varphi} \tag{2.28}$$

This is true if the phase-relaxation time is of the same order or shorter than the momentum relaxation time, that is, if $\tau_{\varphi} \sim \tau_{\mathrm{m}}$, which is often the case with high-mobility semiconductors.

2.5 Scattering in one dimension

It is possible to relate the transport properties of phase coherent one-dimensional conductors to the scattering properties of the electron wavefunctions. Here, we will state the scattering problem for the case where only a single subband is occupied. It is possible to extend these ideas to more than one subband (the "multichannel case") but we are not going to use these in this thesis.

We are going to assume that the electrons see a potential $V(x)$, which is created through confinement as explained above, but it also includes the potentials of space charges and gates. We are going to denote the electron wavefunctions by $\psi(x)$, instead of the notation $\phi_1(x)$ which has been used in section 2.3. We are also going to suppose that the potential $V(x)$ is constant outside a certain interval which we are going call the scattering region. Let V_L be the potential on the left side of the scattering region and V_R be the potential on the right. We are interested in the solution of the Schrödinger equation

$$\left(-\frac{\hbar^2}{2m^*}\frac{\partial^2}{\partial x^2} + V(x)\right)\psi(x) = E\psi(x) \quad , \tag{2.29}$$

and we will assume that the energy eigenvalue E is greater than both V_L and V_R. In other words, the electrons are free at both sides of the scattering region. In that case, the Schrödinger equation can be solved on both of these sides very simply as

$$\psi(x) = \frac{1}{\sqrt{k_L}}\left(Ae^{ik_Lx} + Ce^{-ik_Lx}\right) \quad , \quad x \text{ is on left side} \tag{2.30}$$

$$\psi(x) = \frac{1}{\sqrt{k_R}}\left(De^{ik_Rx} + Be^{-ik_Rx}\right) \quad , \quad x \text{ is on right side} \tag{2.31}$$

where $k_{L,R}$ are the wavenumbers at the left and right of the scattering region

$$k_{L,R} = \sqrt{\frac{2m^*}{\hbar^2}(E - V_{L,R})} \quad . \tag{2.32}$$

The inverse square root factors of wavenumbers are inserted into the wavefunction for later convenience.

As there are only two linearly independent solutions of the Schrödinger equation, only two of the amplitudes A, B, C and D are independent, the other two being dependent on the former two. We would like to express these relationships between

outgoing amplitudes, C and D and the incoming amplitudes, A and B.

$$C = rA + t'B \quad , \tag{2.33}$$

$$D = tA + r'B \quad , \tag{2.34}$$

which can also be written as a matrix equation

$$\begin{bmatrix} C \\ D \end{bmatrix} = S \begin{bmatrix} A \\ B \end{bmatrix} \quad , \tag{2.35}$$

where the coefficient matrix

$$S = \begin{bmatrix} r & t' \\ t & r' \end{bmatrix} \tag{2.36}$$

is called the scattering matrix of the system.

The two particular solutions of the Schrödinger equation corresponding to $A = 1$, $B = 0$ and $A = 0$ and $B = 1$ are called the left incident and right incident scattering wavefunctions, φ_L and φ_R respectively. They have the following limiting form on the left and right sides of the scattering region

$$\varphi_L(x;E) = \begin{cases} \frac{1}{\sqrt{k_L}}\left(e^{ik_Lx} + re^{-ik_Lx}\right) & x \text{ is on left} \\ \frac{1}{\sqrt{k_R}}\left(te^{ik_Rx}\right) & x \text{ is on right} \end{cases} \tag{2.37}$$

$$\varphi_R(x;E) = \begin{cases} \frac{1}{\sqrt{k_L}}\left(t'e^{-ik_Lx}\right) & x \text{ is on left} \\ \frac{1}{\sqrt{k_R}}\left(e^{-ik_Rx} + r'e^{ik_Lx}\right) & x \text{ is on right} \end{cases} \tag{2.38}$$

In accordance with this, t is called the transmission amplitude from left to right, r is called the reflection amplitude from left etc. We can express the general solution in Eqs. (2.30,2.31) as a superposition of these two particular solutions

$$\psi(x) = A\varphi_L(x;E) + B\varphi_R(x;E) \quad . \tag{2.39}$$

Current Conservation: The scattering amplitudes are related to the transmission and reflection probabilities of left and right incident wavepackets, which are formed as superpositions of φ_L or φ_R over a small energy range ΔE. However, it is possible to derive these probabilities without investigating wavepacket behavior by simply invoking the current conservation idea for a definite value of E. The continuity equation

$$\frac{\partial \rho}{\partial t} + \frac{\partial J}{\partial x} = 0 \quad , \tag{2.40}$$

is well-known to be satisfied, where the current density J and the density ρ is given as

$$J = \frac{\hbar}{2m^* i}\left(\psi^* \frac{\partial \psi}{\partial x} - \frac{\partial \psi^*}{\partial x}\psi\right) \quad , \tag{2.41}$$

$$\rho = |\psi|^2 \quad . \tag{2.42}$$

Since the wavefunction ψ has a definite energy, both of J and ρ are time independent. In that case the continuity equation (2.40) is transformed into

$$\frac{\partial J}{\partial x} = 0 \quad . \tag{2.43}$$

This implies that the current density has the same value independent of position, $J(x)$ =const., i.e., the current conservation.

When the current conservation equation is applied to the general solution given in Eqs. (2.30, 2.31), and equating the currents on the left and right sides of the scattering region we get

$$J_L = \frac{\hbar}{2m^*}(|A|^2 - |C|^2) = \frac{\hbar}{2m^*}(|D|^2 - |B|^2) = J_R \quad . \tag{2.44}$$

This equation can be written as

$$|C|^2 + |D|^2 = |A|^2 + |B|^2 \quad , \tag{2.45}$$

which can be interpreted to mean that the incident currents are equal to the outgoing currents. Applying this general result to the two particular solutions we obtain

$$|r|^2 + |t|^2 = 1 \quad , \tag{2.46}$$

$$\left|r'\right|^2 + \left|t'\right|^2 = 1 \quad . \tag{2.47}$$

From these equations, we derive the probability interpretation: $T = |t|^2$ is the transmission probability and $R = |r|^2$ is the reflection probability of the left incident waves, similarly for the right incident ones. Also, the probability is conserved: $R + T = 1$.

Inserting the equation (2.45) into (2.35), we can conclude that the scattering matrix S is unitary,

$$S^\dagger S = S S^\dagger = I \quad . \tag{2.48}$$

From the unitarity of S, it is possible to see that the transmission and reflection probabilities does not depend on whether the particle is incident from left or right, i.e., $T = |t|^2 = |t'|^2$ and $R = |r|^2 = |r'|^2$.

Time reversal symmetry: Another powerful relation involving the scattering matrix can be obtained by using the time reversal symmetry of the Schrödinger equation. This symmetry operation is carried out by taking the complex conjugate of the wavefunction $\psi \longrightarrow \psi^*$ and as long as there is no external magnetic field applied to the system, ψ^* provides another possible solution of the same Schrödinger equation. For the general solution given in Eqs. (2.30, 2.31), the time reversal operation can be carried out on the amplitudes as $A \rightarrow C^*$, $C \rightarrow A^*$ etc. This operation basically exchanges the incoming amplitudes with the outgoing ones together with complex conjugation. As these amplitudes provide another possible solution, they are related by the same scattering matrix as follows

$$\begin{bmatrix} A^* \\ B^* \end{bmatrix} = S \begin{bmatrix} C^* \\ D^* \end{bmatrix} \quad , \tag{2.49}$$

Using Eq. (2.35) again, we get $SS^* = I$. This implies that $S^* = S^\dagger$ and by complex conjugating we finally reach to the result that S is symmetric: $S = \tilde{S}$ where tilde means matrix transpose. For the one-dimensional case we have here, this relation basically tells us that the left and right incidence transmission amplitudes are equal

$$t = t' \quad . \tag{2.50}$$

This relation can easily be extended to the multichannel case as well. As a result, not only the transmission probabilities are equal, but also the amplitudes as well.

2.6 Landauer-Büttiker formalism

The relationship between the scattering and transport properties of one-dimensional phase coherent wires is first stated by Landauer[6] and later generalized to the multichannel case[7]. A very simple derivation of this relation is as follows. We consider the linear regime where a small potential difference ΔV is applied on the two reservoirs (2DEG) on the left and right sides of the wire. The chemical potentials on the left and right then satisfy $\mu_L - \mu_R = (-e)\Delta V$.

We then proceed to compute the current that flows through the wire. We are going to assume that the temperature is very low so that all left incident states below energy μ_L is occupied and all states above it are empty. Similarly for the right incident states. It is easy to see that when the corresponding states on both sides of

the wire is occupied there is no net current, as a result, we only need to consider the states having energy between μ_L and μ_R only (i.e., a small interval around the Fermi level). Suppose the length of the wire is L. The current carried by a single electron is

$$(-e)\frac{1}{L}\nu_F \quad , \tag{2.51}$$

where ν_F is the Fermi velocity. However, the electron will pass to the other side with a probability $T = |t|^2$ so we have to multiply the expression above with this. The total number of such electrons is $N(E_F)\Delta\mu$ where $N(E_F)$ is the density of states at the Fermi level

$$N(E_F) = 2\frac{L}{2\pi}\frac{dk}{dE} = \frac{L}{\pi}\frac{1}{\hbar\nu_F} \quad , \tag{2.52}$$

where the spin factor is included. Therefore the total current is

$$I = (-e)\frac{1}{L}\nu_F\, T\, \frac{L}{\pi}\frac{1}{\hbar\nu_F}\,(-e)\Delta V = \frac{e^2}{\pi\hbar}T\Delta V = 2\frac{e^2}{h}T\Delta V \quad . \tag{2.53}$$

The Fermi velocity has nicely dropped out from the expression, leaving behind a relation that involves only the scattering probability T together with fundamental constants. The conductance of the wire can then be expressed as

$$G = \frac{I}{\Delta V} = 2\frac{e^2}{h}T \quad . \tag{2.54}$$

Note that here T is the transmission probability at the Fermi level.

It should be noted that this expression is the conductance between the two large reservoirs that are connected to the wire and not the conductance of the wire itself. The latter can also be computed, however there is no way to measure them. Basically, the contacts between the reservoirs and the wire also contribute a resistance to the wire which sums up to the final expression given in (2.54). In here, we have also used the assumption that the contacts are reflectionless, i.e., any wavepacket travelling on the wire heading towards contacts is totally transmitted to the reservoirs without any reflection.

This relation can be generalized to the multichannel case where more than one subband is occupied [7]. In that case one has to compute the transmission probabilities T_{mn} from subband n on the left to subband m on the right. The total transmission probability for waves incident in subband n is then $T_n = \sum_m T_{mn}$. The conductance of the wire can then be computed as

$$G = 2\frac{e^2}{h}\sum_n T_n \quad , \tag{2.55}$$

where the sum is over the occupied subbands and again the transmission probabilities are evaluated at the Fermi level. In most cases where the scattering potential $V(x)$ changes slowly with position, the transmission probabilities are very nearly equal to 1, so that in this case the conductance becomes

$$G = 2\frac{e^2}{h}N \quad , \tag{2.56}$$

where N is the total number of occupied subbands, i.e., quantization of conductance. In point contacts defined through a top gate, it is possible to change the number N and in this way it has been possible to observe that the conductance changes between one quantum to another defining flat plateaux [8, 9].

CHAPTER 3

EXPERIMENTS

3.1 Conductance fluctuations in quantum dots

In an experiment a small bias between the electron reservoirs is applied and the voltage drop over the device is measured to compute the conductance. The conductance is measured as a function of a magnetic field, B, applied perpendicular to the plane of the 2DEG. Classically, the magnetic field causes the electrons to move along cyclotron orbits (illustrated in the inset to Fig. 3.1) with radius $r = m^*\nu_{\rm F}/eB$. Due to this perturbation, the transmission probability varies on a characteristic magnetic field scale, $B_{\rm C}$, the field at which the cyclotron diameter equals the side length of the equilateral triangle (for the device used in Fig. 3.1, $B_{\rm C} \approx 50$ mT). The experimental data represented as a dashed line in Fig. 3.1 were taken at a temperature of $T = 4.5$ K, cold enough to be in the ballistic regime where undisturbed trajectories such as the one shown in Fig. 3.1 are possible. At this temperature the data lend themselves to a classical interpretation, and the global maximum of the resistance around $B = B_{\rm C}$ in Fig. 3.1 can be related to the high probability of backscattering of trajectories similar to the one indicated in the inset [10].

Phase coherence can be "switched on" experimentally by lowering the electron temperature below $T \approx 1$ K. Inelastic electron-electron interaction, known to destroy electron wave coherence, is then suppressed, and the edge of the Fermi distribution is sufficiently sharp to resolve effects related to energy quantization. The solid line in Fig. 3.1 shows magneto-resistance data taken at $T = 0.3$ K [5]. Superimposed

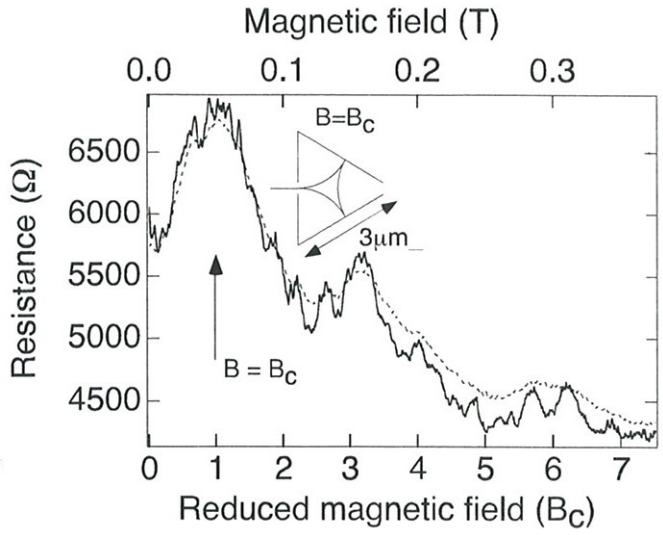

Figure 3.1: The electrical resistance of a triangular cavity measured as a function of a magnetic field. The field is applied perpendicular to the cavity and causes the electrons to move along circular cyclotron orbits (see inset). At a few Kelvin (dashed line, $T = 4.5$K) one can understand the main features of the resistance in terms of classical single-particles trajectories. In the phase-coherent regime (solid line, $T = 0.3$K) electron interference establishes itself as conductance fluctuations superimposed on the classical behavior (From [5]).

on the classical behavior (dashed line) rapid fluctuations are observed on a magnetic field scale of a few mT and less, much smaller than the scale for classical behavior, $B_{\mathrm{C}} \approx 50$ mT.

Since these magneto-conductance fluctuations are observed at a temperature where the wave behavior of the electrons persists and the length scales of scattering are larger than the lateral dimensions of the device, the origin of magneto-conductance fluctuations can be explained in a semi-classical picture of electron transport in which a quantum-mechanical phase is added to the classical electron trajectories (These classical electron trajectories might be defined by Bohr-Sommerfeld quantization rule). Electron waves propagating along pairs of classical electron paths can be interfere constructively or destructively. An external magnetic field shifts the electron phase and changes the interference. In particular, an electron state related to a specific closed orbit will be periodically "switched on and off" as the magnetic field is tuned, with period $\Delta B = h/eA$, given by the ratio of the orbit area, A, and the magnetic flux quantum, h/e. Therefore, the transmission probability, $t(\varepsilon)$, of the electrons oscillates

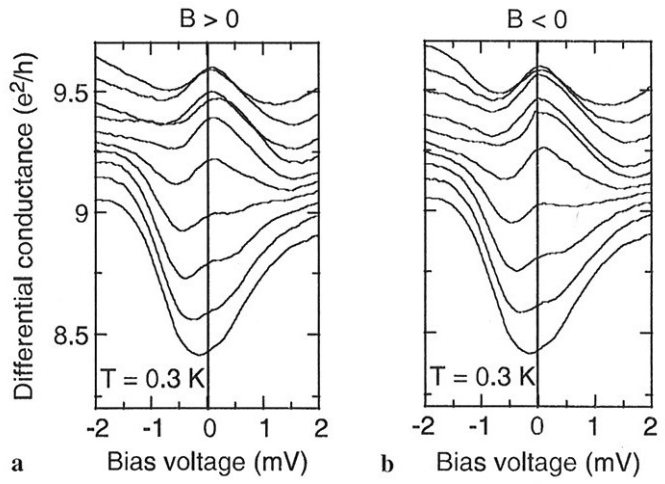

Figure 3.2: Experimental data for the differential conductance, $\partial I/\partial V$, of a triangular electron cavity at increasing perpendicular (a) positive and (b) negative (reversed) magnetic field and a temperature of 0.3 K (From [11]). The field values from bottom to top are for (a) B=-0.2, +1.8, +3.8,...,+17.8 mT and for (b) B=-0.2, -2.2, -4.2,..., -18.2 mT.

as a function of B with frequency spectrum components ΔB given by the areas of the contributing periodic orbits. Since the conductance through the device is proportional to the transmission probability, it will display the same oscillations with the magnetic field. This is the source of the magneto-conductance oscillations.

3.2 Quantum-dot ratchets

In this experiment, a single triangular electron cavity was used (Fig. 1.3a). There are electron reservoirs on both sides of the cavity. These reservoirs became source and drain alternatively during the experiment. In other words, an ac voltage has been applied. So, by the definition made in chapter 1, quantum-dot ratchets are rocking ratchets [2].

To observe a ratchet effect, a small ac voltage of frequency 10-100 Hz, was added to a dc bias voltage, V, and the differential conductance, $\partial I/\partial V$, was measured as a function of V. The resultant data is shown in Fig. 3.2, which was recorded at a series of different (uniform) magnetic fields, which is applied perpendicular to the cavity, ranging from zero to about $\pm$18 mT (Fig. 3.2 (a) and (b), respectively), in steps of 2 mT. The sign of the magnetic field refers to the direction of the field. The following

observations can be made after the careful examination of the graphs shown in Fig. 3.2.

Firstly, it is evident that the graphs are not symmetric with respect to the axis of zero bias voltage. Hence I(-V) $\neq$ -I(V) (non-linear response), which implies that there is a rectification. A more detailed analysis shows that most of the asymmetric behavior is suppressed at temperatures above 1 K.

Secondly, non-linear effects change rapidly with magnetic field. Significantly, the magnetic field scale of these changes (a few mT and less) is the same as that of magneto-conductance fluctuations. This scale is therefore consistent with magnetic-field-induced modifications to quantum interference but not with classical effects (field scale 10-100 mT). Then we can come to the conclusion that the rectifying behavior is due to the voltage-induced modification of transport through electronic quantum states inside the dot.

Third important observation is about the symmetry of the (differential) conductance (G) with respect to zero magnetic field, that is, "magnetic inversion symmetry". This symmetry allows us ensure that the origin of rectification in the device is indeed the geometry and not, for example, broken symmetry because of random impurities of the material (Rectification due to impurities in mesoscopic devices has been observed previously). If the rectification is due to the geometry, then the conductance in the non-linear regime should be symmetric with respect to zero magnetic field. This is because magnetic inversion symmetry (i.e. G(V, -B)=G(V, B)) is possible only when the potential, which the 2DEG is subjected to, has a symmetry axis parallel to the current direction. Otherwise symmetry in magnetic field is normally absent in the non-linear regime. If the rectification is originated from the geometry, then electrons passing through the device does indeed "feel" the triangular shape of the device, which has a symmetry axis parallel to the current direction. Therefore, the equation G(V, -B)=G(V, B) should be satisfied for some range of V and B. On the other hand, if the conductance does not have symmetry in magnetic field, the potential does not have a symmetry axis parallel to the current direction either, which means that the "effective geometry" is different from the dot geometry. The data shown in Fig. 3.2 confirm that the non-linear quantum conductance is independent of the direction of the magnetic field, within a field range that fully alters the non-linear conductance

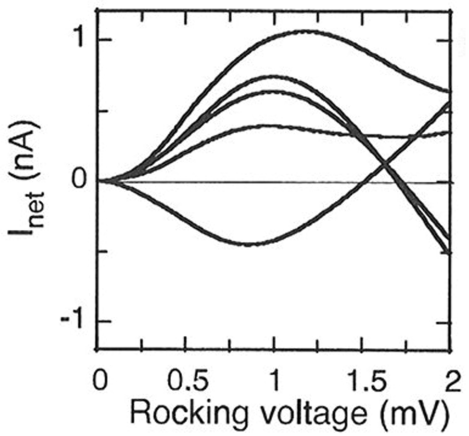

Figure 3.3: The net current generated in a quantum dot ratchet by an ac rocking voltage for different carrier concentrations (Fermi energies) in the 2DEG. Note that the net current direction can be tuned by varying the Fermi energy or the rocking amplitude (From [2]).

fluctuations. Hence it appears that any deviations from the intended dot symmetry are not significant within the parameter range covered here ($|B| < 20$ mT, $|V| < 2$ mV) and the rectification is indeed due to the asymmetric device shape.

Although the relation between the existence of rectification and device shape is observable, it is not a trivial one. This non-trivial relation makes it very difficult to predict precisely the direction of rectification of a given device. The reason is that electron-wave interference is extremely sensitive to variations of the Fermi energy and to the exact distribution of charges forming the electrostatic potential. Nevertheless, it is easy in an experiment to adjust the direction of rectification, once it is established. The current direction can be controlled by modifying the electron states inside the dot using any of the following experimental variables: the device shape (using an external gate), the Fermi energy (using a top-gate, see Fig. 3.3) or a small magnetic field (Fig. 3.2). Moreover, reversal of the current direction can be obtained by using the amplitude of the applied ac voltage (Fig. 3.3).

3.3 Tunneling ratchets

This section contains a review of a ratchet experiment that utilizes tunneling through an asymmetric energy barrier. Temperature-dependent ratchet current direction is

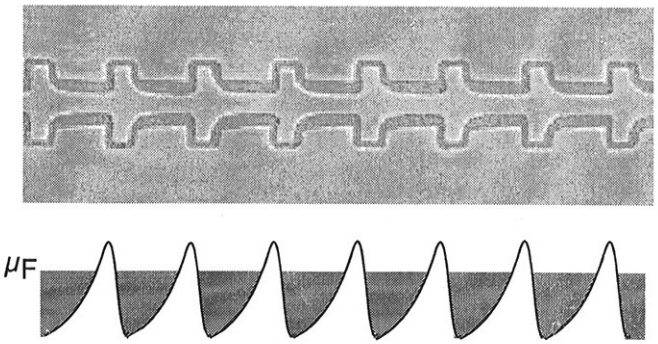

Figure 3.4: An electron tunneling ratchet. *Top*: Scanning electron micrograph; darker areas are etched trenches patterned by electron beam lithography and shallow wet etching. By electrically interrupting a two-dimensional electron sheet located below the device surface, they form an electron-wave guide. *Bottom*: Ratchet potential experienced by 1D electrons moving along the wave guide
(From [2])

the key observation.

A top-view scanning electron micrograph of a tunneling ratchet for electrons is depicted in Figure 3.4. It is an array consisting of ten electron cavities. Etched trenches, visible as darker lines in the image, electrostatically deplete the 2DEG situated about 100 nm underneath the device surface, confining the electrons to a narrow channel with asymmetric, funnel-like constrictions. The lithographic width of this channel is about 100 nm at the narrowest points, corresponding to just a few electron Fermi wavelengths ($\lambda_F \approx 40$ nm). So the channel effectively forms a 1D electron wave guide. In addition, due to the lateral confinement energy, an electron moving along the channel experiences each of the periodic constrictions as an asymmetric energy barrier. The width of the channel (and thus the height of the energy barriers) can be varied by charging the electron sheet regions parallel to the channel using these regions as side-gates. Fig. 3.4 also shows the energy variations of the conductance band bottom (the lowest 1D wave mode) along the channel when the narrowest parts of the channel are only about $\lambda_F/2$ wide, such that the confinement energy at these points is of the order of the Fermi energy. Then there are two possibilities of transport in the channel: by thermal excitation, or by tunneling through the barriers. The lateral dimensions of each cell (i.e. cavity) ($\approx 1\mu$m) were much smaller than the length scales for elastic (6 μm) and inelastic ($> 10\mu$m) scattering at the temperatures

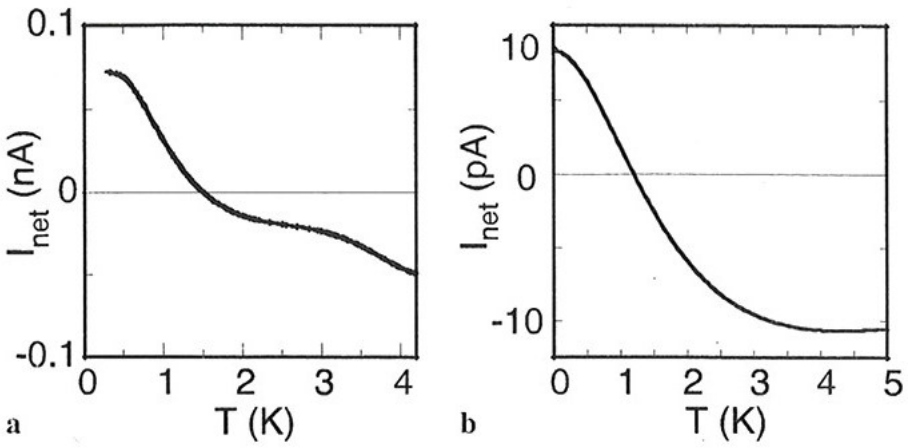

Figure 3.5: (From [2])(a) Measured net electric current, induced by "rocking" the ratchet potential in Fig. 3.4 by a square-wave voltage of amplitude 1 mV, versus temperature. (b) Calculated data of the net current for a rocking voltage of amplitude 0.5 mV and Fermi energy 11.7 meV.

and voltages used here (energies kT and $|eV| \leq 1$ meV) [2].

Contact pads (not visible in Fig. 3.4) situated far away to the left and right of the channel provide electrical access to the 2DEG. Using these contacts as source and drain contacts, a voltage can be applied along the channel. A square-wave source-drain voltage of amplitude V_0 was used to "rock" the ratchet. The frequency was of the order of 100 Hz, which is much slower than all electronic time scales, such as energy relaxation times (adiabatic rocking). The electronic system was therefore in a steady state at all times, and to understand the ratchet behavior it is sufficient to analyze the two dc situations V_0 and -V_0 [2].

In the experiment, to detect a temperature-dependent response in a tunneling ratchet, the barrier height was set to approximately match the Fermi energy, μ_F = 11.8 meV (relative position of barrier height and Fermi energy can be estimated from the conductance of the point contact). Furthermore, the rocking voltage, V, is chosen such that, by varying T, the width of the Fermi window, about ($|eV|$ + $4kT$), can be varied over the energy range around the barrier top where quantum corrections to the transmission probability are important. Then temperature-dependent reversal of current direction in a tunneling ratchet can be observed by sweeping the temperature, while all the other parameters, including the shape and height of the potential barriers, are kept constant. The data shown in Fig. 3.5**a** were obtained using a rock-

ing voltage, V_0=1 mV, corresponding to a voltage drop of 0.1 mV over each barrier (less than 1% of μ_F) in the device shown in Fig. 3.4. The net current generated by this process, I_{net}, corresponds to about 1 to 5% rectification of the total current and, at 4 K, was initially positive but reversed its direction when the temperature was reduced to 0.4 K [2].

CHAPTER 4

THEORY

4.1 Quantum-dot ratchets

How can we use quantum dots to realize a rocking ratchet? To answer this question, one needs to identify mechanisms by which electron interference in quantum dots induce a non-linear current-voltage dependence. Consider first the limit of small voltages (linear response). Figure 4.1a shows schematically the bottom of the conduction band (the lowest allowed electron energy) along the symmetry axis of a triangular quantum dot. The variation of the band represents the confinement energy in the point contacts and inside the dot. The bias voltage is assumed to be negligible, such that there is no potential drop between the chemical potentials (visible as the maximum occupied energies) in the source and drain reservoirs. At very small voltages ($|eV| \ll \mu_{\mathrm{F}}, kT$), transport through the dot is via the electron states within a few kT of the Fermi energy. In this regime, the equation

$$I = GV \tag{4.1}$$

is valid, where

$$G = (2e^2/h)M(\mu_{\mathrm{F}})t(\mu_{\mathrm{F}}) \tag{4.2}$$

does not depend on voltage and μ_F is the equilibrium Fermi energy, where M is the number of conducting sub-bands and t is the average transmission probability over these sub-bands [1]. The electron states inside the dot contributing to the current are those at the Fermi energy and are the same for both current directions, such that

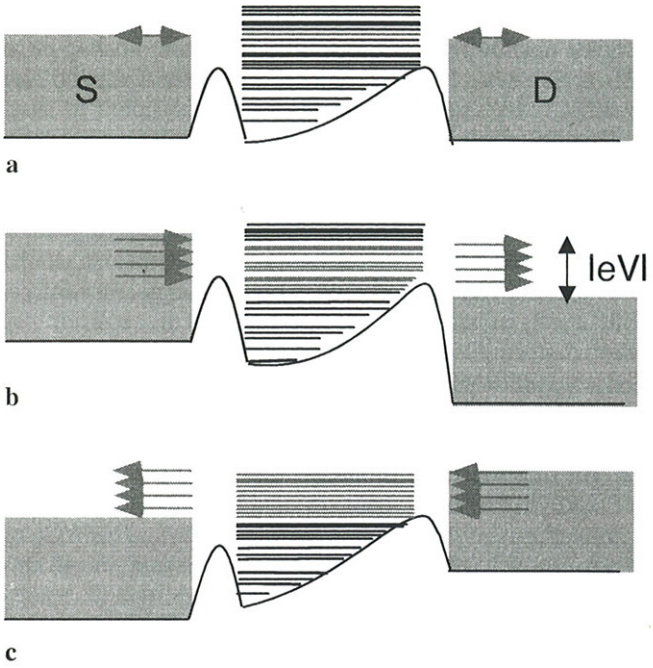

Figure 4.1: Illustration of electron transport through a quantum dot (From [2])

conductance is symmetric.

The quantum-dot band structure for finite voltage is shown in Fig. 4.1b,c. The potential drop between the reservoirs distorts the 2D dot potential, U, and therefore changes the exact configuration of electron states inside the dot [11, 12]. Because of the asymmetry, the distortion depends, in general, on the sign of the voltage ($U(V) \neq U(-V)$), such that different sets of electron states inside the dot carry the current depending on the current direction. As a result, $t(\varepsilon, U(V))$ depends on the sign of the voltage, causing non-linear and non-symmetric behavior of the conductance. As a second effect, a finite bias voltage increases the width of the Fermi window, $[f_{\mathrm{S}}(\varepsilon) - f_{\mathrm{D}}(\varepsilon)]$, which describes the energy range over which electrons contribute to the conductance. The exact position of this window relative to the conductance band bottom inside the dot depends on how the voltage drop is distributed over the device [13]. When the two point contacts are different, as is necessarily the case for a triangular quantum dot, a different range of quantized electron states will contribute to the current for the two signs of the voltage.

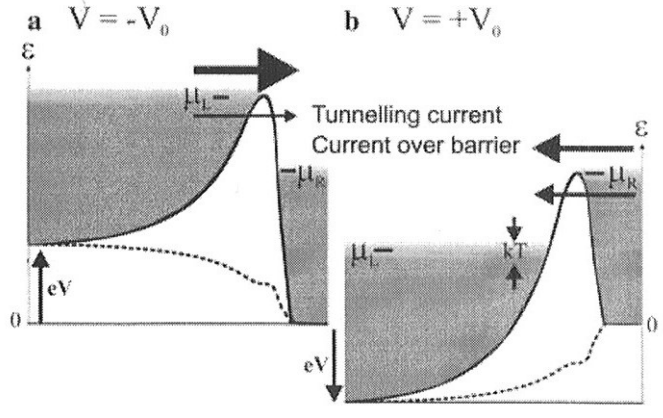

Figure 4.2: Model of a single ratchet barrier of the device in Fig. 3.4 (From [2]). The shape of the barrier is based on the lithografic shape of the electron wave guide and has a maximum barrier height of 12 meV at zero bias. To obtain the barrier at finite negative (a) or positive (b) voltage, an assumption for the spatial distribution of the voltage drop needs to be made (dashed line). The arrows indicate the flow directions of electrons (electron flow from right to left corresponds to positive electrical current).

4.2 Tunneling ratchets

The observed reversal of the current direction as a function of temperature can be explained intuitively by considering how the shape of the energy barriers deforms in an electric field and how this change affects electron transmission. In Fig. 4.2 we show estimated barrier shapes for the device in Fig. 3.4 for negative (Fig. 4.2a) and positive (Fig. 4.2b) bias voltage applied to the left reservoir. In each case, the flow of electrons is "downhill" as indicated by the arrows. Crucially, however, when the barrier is tilted to the right ($V < 0$), it deforms to be thicker at a given energy under the barrier top than when tilted to the left ($V > 0$). Consequently, the energy composition of the current is different for $V > 0$ and $V < 0$: a thicker barrier reduces the probability for tunneling through the barrier, but, at the same time, makes it easier for electrons with high energy to cross over the barrier, because the smoother shape reduces wave reflection. Smoothness of the barrier is important because this ratchet is essentially a 1D wave guide, and any rapid spatial change of the potential leads to partial wave reflection even when the electron has enough energy to pass above the barrier. The electron flow above the barrier is thus larger for $V < 0$ than for $V > 0$, while the flow of electrons that tunnel through the barrier is larger for

$V > 0$ than for $V < 0$. Averaged over a full period of symmetric rocking, there is a net particle current to the left consisting of electrons with low energy that tunnel through the barriers. At higher energy, a net current flows to the right, consisting of electrons that pass over the top of the barrier. The direction of the total, energy-averaged net current, I_{net}, depends then on the electron energy distribution. At high temperatures, the current to the left (negative electrical current) will usually dominate, because electrons of higher energy are available. As the temperature decreases, however, this contribution can become smaller than the tunneling current, and a reversal of the total net current can be observed.

To quantitatively model the net current as a function of temperature, we assume that transport across each energy barrier is ballistic and no inelastic processes occur (that is, the electrons do not change their energy while traversing the barrier), and we consider electron transport in the lowest 1D wave mode only, assuming that any higher 1D wave modes are not populated at the narrowest points of the wave guide. The electric current driven by a bias voltage, V, applied between the 2DEG reservoirs at either end of the channel is

$$I(V) = \frac{2e}{h} \int_0^\infty t(\varepsilon, V)[f_{\mathrm{L}}(\varepsilon, V) - f_{\mathrm{R}}(\varepsilon, V)]d\varepsilon \tag{4.3}$$

Here,

$$f_{\mathrm{L/R}}(\varepsilon, T) = 1/\{1 + \exp[(\varepsilon - \mu_{\mathrm{L/R}})/kT]\} \tag{4.4}$$

are the Fermi distribution functions in the electron reservoirs to the left (L) and right (R) of the barrier. $t(\varepsilon, V)$ is the probability that electrons are transmitted through the device. We assume that $(|eV|, kT) \ll \mu_{\mathrm{L/R}}$, which allows us to use zero as the lower limit of integration, independent of the voltage sign.

To find the current at a given bias voltage, we need to calculate the transmission function, $t(\varepsilon)$, of the barrier at that voltage The form of the energy barriers at zero bias voltage can be estimated from the lithographic shape of the channel and lateral electron confinement energy (Fig. 3.3;for details see [12]). To obtain the barrier shape at finite voltage, the spatial distribution of the potential drop between reservoirs needs to be known, which self-consistently depends on screening effects. Here we assume a spatial distribution of the voltage drop that is proportional to the local derivative of the barrier (Fig. 4.2). This model is based on the notion that a more rapid potential

variation leads to stronger wave reflection, and therefore a more rapid local voltage drop [13]. This particular choice has the side effect that the barrier changes with voltage in a symmetric manner, resulting in the suppression of a classical contribution to the net current.

Once the barrier shapes at $V > 0$ and $V < 0$ are known, the transmission $t(\varepsilon)$ is calculated for each of the two voltages by solving the 1D Schrödinger equation, and the dc current for each voltage can be calculated. The (time averaged) net current induced by a square-wave voltage switching between $\pm V_0$ can be written as follows:[12]

$$I_{\rm net}(V_0) = \frac{e}{h}\int_0^\infty \Delta t(\varepsilon, V_0)\Delta f(\varepsilon, V_0)d\varepsilon \tag{4.5}$$

where

$$\Delta f(\varepsilon, V_0) \equiv [f_{\rm L}(\varepsilon, V_0) - f_{\rm R}(\varepsilon, V_0)] \tag{4.6}$$

is the "Fermi window", the range of electron energies which contribute to the current. The term

$$\Delta t(\varepsilon, V_0) \equiv [t(\varepsilon, V_0) - t(\varepsilon, -V_0)] \tag{4.7}$$

is the difference between the transmission probabilities for positive and negative voltages.

4.3 A model and corresponding numerical scheme applicable to the rocking quantum-dot ratchet

We are interested in solving the transport problem under nonlinear conditions. Here we describe the problem and the method of solution based on the formalism described at the end of chapter 2, and also on the assumption that the transport is coherent and that the electrons move in the ballistic limit.

The geometry of the problem is shown in Fig. 4.3. The system consists of two reservoirs containing 2DEG, and leads that contain a scattering region in the middle. For example, the scatterer might be the triangular cavity shown in Fig. 1.3. The device, that is the cavity, will also be called "the scatterer" in this section. Scattering of electron waves in the device region is important for the determination of the currents. We will assume that the leads are uniform in size having constant potential. That way no scattering takes place in the leads. We will also assume that the leads

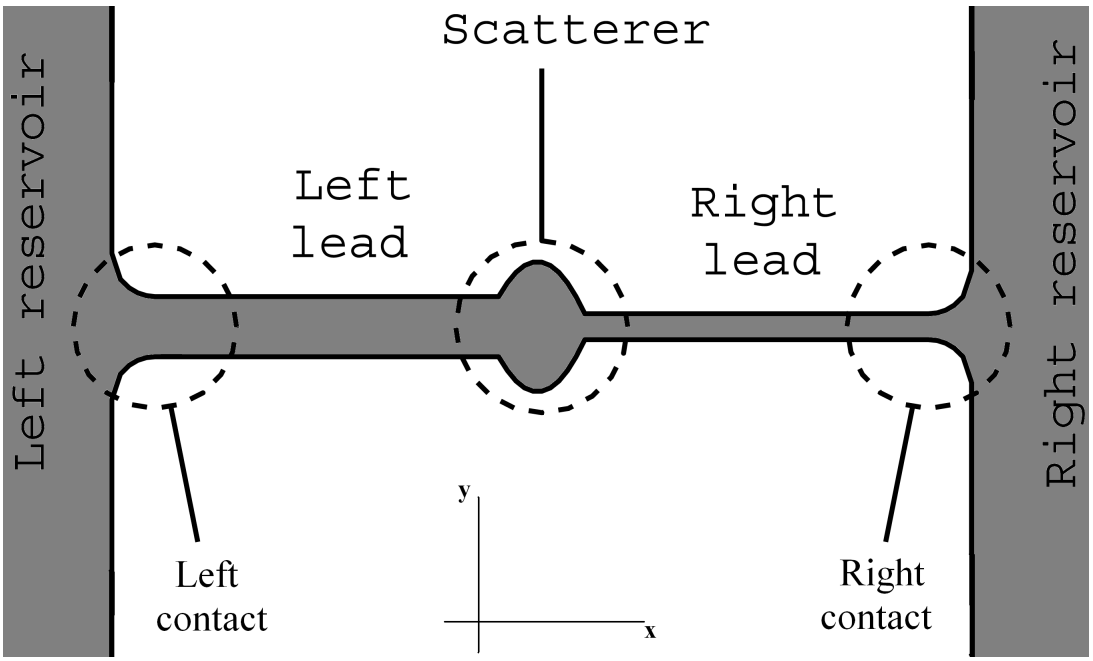

Figure 4.3: Geometry of the scattering problem

are long enough so that changes in the charge distribution around the scatterer will have no effect for parts of the leads sufficiently far away.

To be able to apply external potential differences and measure currents, large macroscopic reservoirs should be connected to the leads. We will assume that the reservoirs are large with large density of states at every energy. The region that leads are connected to the reservoirs are called contacts. We will assume that the contacts are "reflectionless". This essentially means that any wave propagating in the lead and approaching to the contact is completely transmitted to the reservoir with no reflection. Opposite is not true. Waves in the reservoirs incident towards the lead are largely reflected with only a small transmission probability. This difference basically arises from the difference in the number of transverse modes in the reservoir and in the leads at a given energy. The lead has only a finite number of modes (we will assume one), but the reservoir has infinitely many.

Denoting modes in the lead by n and those in the reservoir by α, the transmission amplitude from mode n to mode α is given by $S_{\alpha n}$ where S is the scattering matrix for the contact. We will suppose that there is no magnetic field so that S-matrix is symmetric. In that case we have $S_{n\alpha} = S_{\alpha n}$. The total transmission probability

from mode-n to the reservoir is $T_n = \sum_\alpha |S_{\alpha n}|^2$ and reflectionless contact assumption means that $T_n = 1$ for each n (which also means that $S_{mn} = 0$). Since there are infinite labels α, each $S_{\alpha n}$ has to be very small, i.e., incident wave is distributed to many modes.

On the other hand, when a wave in mode α is incident towards the contact, the transmission probability is $T_\alpha = \sum_n |S_{n\alpha}|^2$ and this is small. Most of the wave is reflected with probability $1 - T_\alpha = \sum_\beta |S_{\beta\alpha}|^2$.

Electron number density can be expressed in terms of the energy eigenfunctions and an appropriate (Fermi-Dirac) distribution function.

$$n(\vec{r}) = 2 \sum_s f_s \, |\psi_s(\vec{r})|^2 \quad , \tag{4.8}$$

where the factor 2 is for spin degeneracy. If the quantum number s is in continuum, we will have an integral instead of a summation. Here f_s is the occupation probability of the level-s. Fermi-Dirac distribution has to be used naturally for the value of f_s but its determination will be discussed below.

An important principle that we will use is that the charge density in the reservoirs and the leads should not change when external potentials are applied to the system. This is due to the charge neutrality condition that needs to be satisfied exactly. However, the charge density around the contacts and the scatterer will change. Changing density will imply a changing potential profile in these regions. What we want to do in here is to determine the changes in the potential profile so that the scattering problem can be solved self consistently.

From the charge neutrality condition we can conclude that the potentials inside the reservoirs and the leads remain flat. However their values might be shifted up or down. We are going to denote the potentials of the reservoirs by W_L and W_R and those in the lead by V_L and V_R. Although these values change when external potential differences are applied, we will assume that the reflectionless contacts assumption is still valid.

Next, we note that the reservoirs are very large. For that reason, local electronic properties (local charge density, current density, etc.) should not depend on the presence of the device and the current passing on it. There is a current density going towards or coming from the contacts but with the assumption that the width of the reservoir is infinitely large, these differences will be negligibly small. Far away from

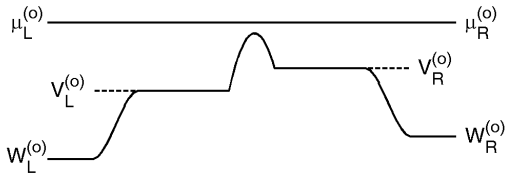

Figure 4.4: The bottom of the bands and Fermi levels under equilibrium conditions.

the contacts, all electronic properties of the reservoir should be unchanged. For that reason, the usual Fermi-Dirac distribution of the levels can be assumed in these regions and therefore each reservoir will have its own chemical potential, μ_L and μ_R. We need to use two different Fermi-Dirac distribution functions $f_L(E)$ and $f_R(E)$ and we can see that these depend only on the energy E of the level.

Since the local electronic properties are unchanged, the differences $\mu_L - W_L$ and $\mu_R - W_R$ should not change when external potentials are applied. Although both μ_L and W_L shifts under changing conditions, they have to shift by the same amount. Similarly for μ_R and W_R.

Once we have $f_L(E)$ and $f_R(E)$, we have the distribution function for almost all levels. This is because all extended states can be thought as waves (i) in the left reservoir incident towards the left contact and (ii) in the right reservoir incident towards the right contact. Any extended wave in the leads and the scattering region can be thought as an extension of these two types of waves. Also note that the waves of type-(i) are mostly present in the left reservoir (incident and reflected parts included) with only a small leakage towards the right reservoir.

The only exception to these rules will be the bound states in the scatterer. However, since these will have very low energy, we can assume an occupation probability of 1 for these. So, no problem is introduced. Only in excessively large applied potential differences where for example μ_R becomes lower than V_R some problems will arise, but in here we are not going to meet such cases.

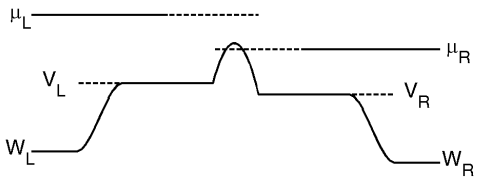

Figure 4.5: The bottom of the bands and Fermi levels under nonequilibrium conditions.

From the local chemical potentials we can determine the applied potential difference as follows: Suppose that when there is no external potential applied, the potential energies (bottom of the bands) are denoted by $W_L^{(o)}$, $W_R^{(o)}$, $V_L^{(o)}$ and $V_R^{(o)}$. Under these conditions, both reservoirs have the same chemical potential $\mu_L^{(o)} = \mu_R^{(o)}$ (See Fig. 4.4). There is a constant potential difference $W_L^{(o)} - W_R^{(o)}$ between left and right reservoirs due to charges redistributed at the contacts and the scatterer.

When an external potential difference $\tilde{V}$ is applied to the left reservoir with respect to the right, $W_L - W_R$ changes by that amount: $W_L - W_R = (W_L^{(o)} - W_R^{(o)}) + (-e)\tilde{V}$. For such a case, the difference between the chemical potentials becomes:

$$\begin{aligned} \mu_L - \mu_R &= (\mu_L - W_L) + (W_L - W_R) - (\mu_R - W_R) && (4.9)\\ &= (\mu_L^{(o)} - W_L^{(o)}) + (W_L - W_R) - (\mu_R^{(o)} - W_R^{(o)}) && (4.10)\\ &= (W_L - W_R) - (W_L^{(o)} - W_R^{(o)}) && (4.11)\\ &= (-e)\tilde{V} \quad . && (4.12) \end{aligned}$$

Therefore, the applied potential difference is directly related to the chemical potential difference (see Fig. 4.5).

4.3.1 The leads and the scatterer

Let us consider the calculation of the charge density in the leads. We have said that any extended wave at energy E in these regions can be considered as a continuation

of waves that originated in the reservoirs. Let $\psi_\alpha(\vec{r}, E)$ represent waves coming from the left reservoir and $\psi'_\alpha(\vec{r}, E)$ represent those coming from the right. We know that the charge density within the leads and the scattering region can be calculated as follows:

$$n(\vec{r}) = 2\sum_\alpha \int dE f_L(E) \left|\psi_\alpha(\vec{r}, E)\right|^2 + 2\sum_\alpha \int dE f_R(E) \left|\psi'_\alpha(\vec{r}, E)\right|^2 \quad (4.13)$$

$$= n^{(left)}(\vec{r}) + n^{(right)}(\vec{r}) \quad , \quad (4.14)$$

i.e., we can separate the charge density into two parts, one arising from left incident waves and other from right incident waves (other electronic properties can be separated in such a way as well).

First consider $n^{(left)}(\vec{r})$. Note that there are only a finite number of modes in the leads so that any wave ψ_α will be a superposition of these finite solutions in the region considered. In other words

$$\psi_\alpha(\vec{r}, E) = \sum_n S_{n\alpha}(E)\varphi_{Ln}(\vec{r}, E) \quad , \quad (4.15)$$

where $S(E)$ is the scattering matrix for the left contact and $\varphi_{Ln}(\vec{r}, E)$ are solutions of the Schrödinger's equation in the region containing leads and the scatterer for left-incident waves. (In other words, these are solutions obtained by assuming infinitely long leads). In the expression no sums over right incident solutions $\varphi_{Rn}(\vec{r}, E)$ are included because this is not possible (the right contact is reflectionless). In such a case we get

$$\sum_\alpha \left|\psi_\alpha(\vec{r}, E)\right|^2 = \sum_n \left|\varphi_{Ln}(\vec{r}, E)\right|^2 \quad , \quad (4.16)$$

where we have used the fact that the S-matrix is unitary and the left contact is reflectionless: $\sum_\alpha S^*_{n\alpha} S_{m\alpha} + \sum_\ell S^*_{n\ell} S_{m\ell} = \delta_{nm}$, $S_{n\ell} = 0$. The final result is simple,

$$n^{(left)}(\vec{r}) = 2\sum_n \int dE f_L(E) \left|\varphi_{Ln}(\vec{r}, E)\right|^2 \quad . \quad (4.17)$$

The simplicity of the result is that when trying to find the charge distribution in the region containing the leads and the scatterer, we don't need to know the scattering matrices of the contacts or other properties of the reservoirs. Only the solution of the Schrödinger's equation in this region is needed (and $\mu_{L,R}$ of course). The same result will be valid for $n^{(right)}$

$$n^{(right)}(\vec{r}) = 2\sum_n \int dE f_R(E) \left|\varphi_{Rn}(\vec{r}, E)\right|^2 \quad . \quad (4.18)$$

As we don't need to know anything about the potential profile around the contacts, the problem is simplified. For this reason, we will assume that the leads are infinite in extent, but the the distribution of electrons are described by two different functions $f_L(E)$ and $f_R(E)$ applied separately to the left incident and right incident waves respectively.

4.3.2 The Problem

First, we describe the leads and the scatterer under equilibrium. At this point we will assume that the problem at hand is a strictly one dimensional one, so that at most one mode will be present in each lead. In other words, only the lowest subband is occupied. The electrons move under a potential profile shown by $V^{(o)}(x)$. This potential varies around the scattering region but it has a flat shape deep into the leads.

$$V^{(o)}(x) \longrightarrow V_L^{(o)} \text{ as } x \longrightarrow -\infty \quad , \tag{4.19}$$

$$V^{(o)}(x) \longrightarrow V_R^{(o)} \text{ as } x \longrightarrow +\infty \quad . \tag{4.20}$$

For simplicity, we might assume that the potential becomes a constant outside a fixed interval (convenient for numerical solutions).

This potential arises from two contributions. One is the confining potential of the leads and the potential that create the device and the other is the Coulomb repulsion of the electrons. In the rectification effect that we are interested in, the change in the charge distribution around the scatterer is the main reason for the change in the potential profile. Therefore, for a realistic calculation, the Coulomb potential has to be computed based on the charge distribution, which itself depends on the potential profile. A self-consistent calculation is needed to solve this problem. However, in this study, we are going to replace this by a very simple model that assumes that the $V(x)$ changes more at places where $V^{(o)}$ changes rapidly [2]. These are the places where the electron reflection is significant and for this reason, the charge distribution is more sensitive to the changes in the potential profile. This model basically assumes that

$$V(x) = V^{(o)}(x) + Us(x) \quad , \tag{4.21}$$

where the derivative $ds(x)/dx$ is taken to be proportional to the derivative $dV^{(o)}(x)/dx$.

We are going to choose $s(x)$ so that $s(-\infty) = 1/2$ and $s(+\infty) = -1/2$. With this, U is basically the change in $V_L - V_R$ difference,

$$V_L - V_R = (V_L^{(o)} - V_R^{(o)}) + U \quad . \tag{4.22}$$

Next, we look at the charge density at the leads. At equilibrium there will be only one Fermi level, $\mu^{(o)}$, and only one distribution function, $f^{(o)}(E)$. The charge-density, then, can be expressed as

$$n^{(o)}(x) = 2\int_{V_L^{(o)}}^{\infty} dE f^{(o)}(E)\,|\varphi_L(x;E)|^2 + 2\int_{V_R^{(o)}}^{\infty} dE f^{(o)}(E)\,|\varphi_R(x;E)|^2 \quad . \tag{4.23}$$

Two important parameters are the charge densities in the deep parts of the leads,

$$n^{(o)}(x) \longrightarrow n_L \text{ as } x \longrightarrow -\infty \quad , \tag{4.24}$$

$$n^{(o)}(x) \longrightarrow n_R \text{ as } x \longrightarrow +\infty \quad . \tag{4.25}$$

These are also going to remain unchanged.

Under nonequilibrium conditions, the chemical potentials μ_L and μ_R are different. Note that $\mu_L - V_L$ and $\mu_R - V_R$ might change but n_L and n_R should be constant. The charge densities of the leads can be calculated from the energy dependent scattering solutions. Consider first the left lead. In this region the scattering states are

$$\varphi_L(x;E) = \frac{1}{\sqrt{hv_L}}\left(e^{ik_Lx} + r(E)e^{-ik_Lx}\right) \quad , \tag{4.26}$$

$$\varphi_R(x;E) = \frac{1}{\sqrt{hv_L}}\,t'(E)e^{-ik_Lx} \quad , \tag{4.27}$$

where k_L is the wavenumber and v_L is the corresponding velocity at the indicated energy. The normalization factor is chosen so that the wavefunctions above form an orthonormal set, i.e., $\langle\varphi_\alpha(E_1) \mid \varphi_\beta(E_2)\rangle = \delta_{\alpha\beta}\delta(E_1 - E_2)$. The charge density at x is then

$$n(x) = 2\int_{V_L}^{\infty} \frac{dE}{hv_L} f_L(E)\left[1 + |r(E)|^2 + r(E)e^{-2ik_Lx} + r(E)^*e^{2ik_Lx}\right] \tag{4.28}$$

$$+2\int_{V_R}^{\infty} \frac{dE}{hv_L} f_R(E)\left|t'(E)\right|^2 \quad . \tag{4.29}$$

First of all, it is convenient to make a change of variable from energy to the wavenumber k_L by using $E = V_L + \hbar^2k_L^2/2m^*$ and note that $dE = \hbar v_L dk_L$. Second, deep into the lead ($x \longrightarrow -\infty$), the oscillatory terms decay to zero. The final result for n_L is

$$n_L = \frac{2}{2\pi}\int_0^{\infty} dk_L f_L(E)[1 + |r(E)|^2] + \frac{2}{2\pi}\int_0^{\infty} dk_L f_R(E)\left|t'(E)\right|^2 \quad . \tag{4.30}$$

The final convenient form is

$$n_L = \frac{2}{2\pi}\left[2\int_0^\infty dk_L f_L(E) + \int_0^\infty dk_L[f_R(E) - f_L(E)]T(E)\right] \quad . \tag{4.31}$$

Basically knowing the transmission probability, $T(E) = |t(E)|^2$, we can calculate the densities n_L and n_R. The expression for the right lead can be obtained in a similar way.

$$n_R = \frac{2}{2\pi}\left[2\int_0^\infty dk_R f_R(E) + \int_0^\infty dk_R[f_L(E) - f_R(E)]T(E)\right] \quad . \tag{4.32}$$

After this point we are going to assume that the temperature is zero so that Fermi-Dirac distribution is a step function. We are going to use four symbols to express the fermi levels in terms of wevenumbers.

$$\mu_L = V_L + \frac{\hbar^2 K_L^2}{2m^*} = V_R + \frac{\hbar^2 Q_R^2}{2m^*} \quad , \tag{4.33}$$

$$\mu_R = V_L + \frac{\hbar^2 Q_L^2}{2m^*} = V_R + \frac{\hbar^2 K_R^2}{2m^*} \quad . \tag{4.34}$$

As a result a level with wavenumber k_L in the left lead is present in left-incident form if $k_L < K_L$ and present in right-incident form if $k_L < Q_L$. In terms of the wavenumber k_R in the right lead, it will be present in right-incident form if $k_R < K_R$ and in left-incident form if $k_R < Q_R$. Note that Q_R is associated with μ_L and vice versa. Also note that

$$K_L^2 - Q_L^2 = Q_R^2 - K_R^2 = \frac{2m^*(-e)\tilde{V}}{\hbar^2} \quad . \tag{4.35}$$

The densities n_L and n_R can now be expressed as

$$n_L = \frac{2}{2\pi}\left[2K_L + \int_{K_L}^{Q_L} dk_L T(E)\right] \quad , \tag{4.36}$$

$$n_R = \frac{2}{2\pi}\left[2K_R + \int_{K_R}^{Q_R} dk_R T(E)\right] \quad . \tag{4.37}$$

Note that in these two equations the integrands are different since $dk_L \neq dk_R$.

Finally, at equilibrium integrals disappear since $Q_L = K_L$ and $Q_R = K_R$. If the wavenumbers are called $K_L^{(o)}$ and $K_R^{(o)}$, the conditions that the charge distribution remain unchanged deep into the leads can be expressed as

$$K_L^{(o)} = K_L + \frac{1}{2}\int_{K_L}^{Q_L} dk_L T(E) \quad , \tag{4.38}$$

$$K_R^{(o)} = K_R + \frac{1}{2}\int_{K_R}^{Q_R} dk_R T(E) \quad . \tag{4.39}$$

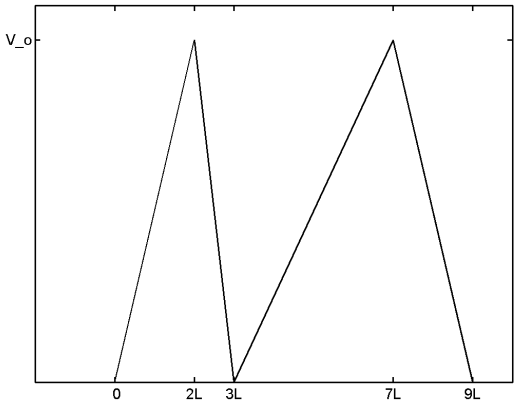

Figure 4.6: The equilibrium potential profile used in this numerical study.

Note that these conditions are implied by the Coulomb interaction between the electrons which naturally leads to screening and the charge neutrality condition. Therefore, Eq. (4.21) together with Eqs. (4.38-4.39) will enable us to determine the potential profile in the scatterer under nonequilibrium conditions. Mathematically, it is more convenient to start with a known value of U, compute from Eqs. (4.38-4.39) the chemical potentials and then determine the externally applied potential $\tilde{V}$, for this reason this method is used below.

Finally we compute the total current flowing from the device by using the Landauer-Büttiker formalism[6, 7] as

$$I = 2\frac{(-e)}{h}\int_{V_L} dE f_L(E)\left|t(E)\right|^2 - 2\frac{(-e)}{h}\int_{V_R} dE f_R(E)\left|t'(E)\right|^2 \quad , \tag{4.40}$$

$$= 2\frac{(-e)}{h}\int_{\max(V_L,V_R)} dE[f_L(E) - f_R(E)]\left|t(E)\right|^2 \quad , \tag{4.41}$$

where we have used the symmetry of the S-matrix, $t(E) = t'(E)$.

4.3.3 The Model

We consider a scatterer formed by two asymmetrical triangular barriers. The potential profile is shown in Fig. 4.6. For each triangle the leftward looking slope has twice more length than the other slope while the second triangle has twice the length of the first. Two triangular barriers have the same maximum at V_0. We choose the left and right limiting potentials to be equal which is set to be zero: $V_L^{(o)} = V_R^{(o)} = 0$. In the following, all quantities will be made dimensionless by using appropriate units

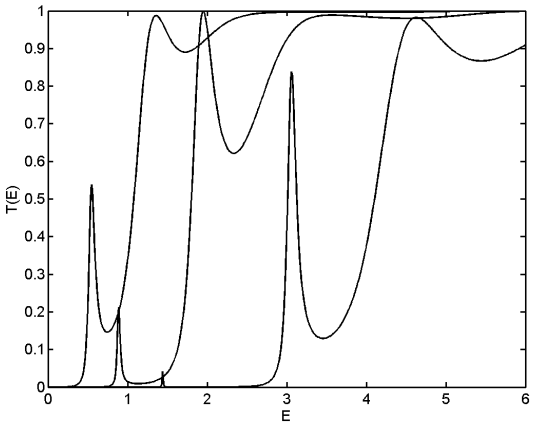

Figure 4.7: The transmission probability versus energy graph under equilibrium for (from top to bottom) $V_0 = 1$, 2 and 4.

for each quantity based on the length scale L of the barriers. All lengths will be expressed in units of L, and all wavevectors in units of $1/L$. The natural unit for the energy is $\hbar^2/2m^*L^2$.

The transmission probabilities for three different values of V_0 are shown in Fig. 4.7. As can be seen, there is a significant interference in the structure. As a result, any change in the potential will alter these curves in different ways, sometimes increasing and sometimes decreasing the transmission probability. Therefore the current-voltage characteristic can be expected to depend significantly on where the Fermi level is.

In Fig. 4.8, the current-voltage ratio is plotted against the applied potential difference for three different values of the equilibrium Fermi level. When the Fermi level is well below the barrier potential V_0, the equilibrium conductance is low. However, with the applied bias, electrons with much higher energies are injected to the system and for this reason the current-voltage ratio tends to increase with the applied bias.

On the opposite extreme, when the equilibrium Fermi level is well above the barrier potential V_0, the transmission probability is very nearly equal to 1 and the equilibrium conductance is already at its maximum. For this reason, under higher bias, it naturally tends to decrease initially. In all cases, it can be seen that these curves are asymmetric under polarity change $\tilde{V} \longrightarrow -\tilde{V}$.

To investigate the rectification behavior, we assume that a square wave pulse is

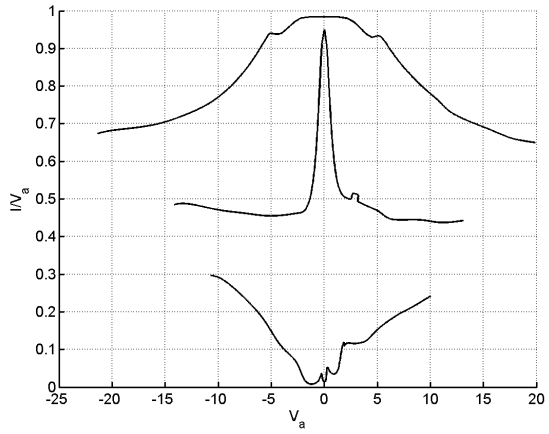

Figure 4.8: The current-voltage ratio $I/\tilde{V}$ is plotted against the applied potential $\tilde{V}$ for $V_0 = 2$ and for three different values of the Fermi energy (from top to bottom) $E_F = 4$, 2 and 1 (applied potential is indicated by V_a in the graph).

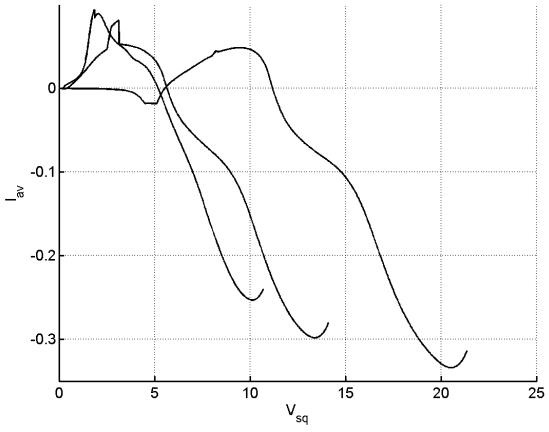

Figure 4.9: The average current plotted against the square wave amplitude when the device is driven by a square wave pulse. The curves are for $V_0 = 2$ and for three different values of Fermi energy, (from top to bottom for $V_{\text{sq}} > 6$) $E_F = 4$, 2 and 1.

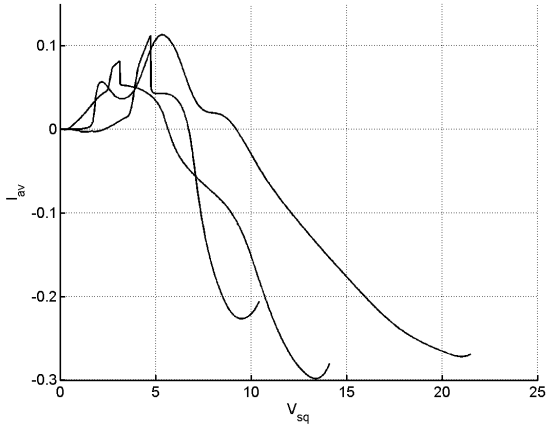

Figure 4.10: The average current plotted against the square wave amplitude when the device is driven by a square wave pulse. The curves are for $E_F = 2$ and for three different values of maximum value of potential, (from top to bottom for $V_{\text{sq}} > 7$) $V_0 = 4$, 2 and 1.

applied to the system. The potential difference periodically changes between $+V_{\text{sq}}$ and $-V_{\text{sq}}$. As the durations of these two potentials are equal, the average current that pass over the barrier (the dc component generated) is given as

$$I_{\text{av}} = \frac{1}{2}\left(I(+V_{\text{sq}}) + I(-V_{\text{sq}})\right) \quad . \tag{4.42}$$

The graph of the average current to the amplitude of the square wave pulse is shown in Fig. 4.9. It can be seen that the average current changes direction when the amplitude of the pulse is increased. Moreover, for the curve $E_F = 4$ there are two successive direction reversals.

Same curves are shown for three different values of V_0 at the same value of the Fermi energy in Fig. 4.10. In that case too all curves show a direction reversal when amplitude is increased. Moreover, for $V_0 = 1$ there are again two successive reversals, but the first one is barely noticeable in the figure.

The direction reversal also occurs when the amplitude V_{sq} is fixed and either the Fermi level or the maximum potential is changed. But, this happens at low or intermediate values of V_{sq}. For sufficiently large values of V_{sq}, the average current appears to be always negative. It implies that for very large bias voltages, the current flow from right to left is larger than the flow from left to right, due to less reflection in the former case.

CHAPTER 5

CONCLUSION

The main objective of this thesis is to review a recently observed phenomenon which was observed in two specific experiments that was performed by using two mesoscopic semiconductor devices (see Fig. 1.3 and 3.4). The phenomenon is called the ratchet effect. These devices are formed at the interface of a so-called an AlGaAs/GaAs heterostructure. This interface contains a two-dimensional electron gas (2DEG) (see Fig. 2.1). At low temperatures ($T < 5$ K), the motion of the electrons through the devices are ballistic and phase coherent. Thus it is possible to describe the motion of an electron by using a plane wave. In this case the current passing through the device is influenced by interference effects. So one can expect a non-trivial response from the devices. The device whose response is dominantly affected by electronic interference is a rocking ratchet. As explained in Chp. 4, particles with energy less than some energy which is determined by width of the contacts by which devices are connected to reservoirs cannot penetrate through the devices except by tunneling. So if such a device is connected to some reservoirs with Fermi energy about that critical value of energy, then the response of this device will be affected by tunneling dominantly. Such devices are called tunneling ratchets. Due to the phase coherence and ballistic motion of electrons (see Fig. 1.3) geometry of such devices become important.

The experiments showed that these devices exhibits a non-trivial behavior. They have non-linear responses to applied bias. Thus they rectify a current generated by an ac voltage. However, this results need interpretation. One must find a theoretical

basis by which the phenomenon can be related to fundamental principles.

To find a theoretical explanation, one must write down the corresponding equation for an electron in a 2DEG (see Chp. 2). It is similar to two-dimensional Schrödinger equation. Now consider an electron moving in a constriction of uniform width, a canal. Another important problem is to model the potential due to the confinement. There are two interesting cases: hard-wall confinement and parabolic confinement. When using hard-wall confinement, the solution is converted into box problem in the transverse direction and free particle in the longitudinal direction. If there is a change in the width, then there is a correlation between the directions of motion. If the energy of the electron is low enough and also there is no abrupt change in the width, then it occupies only the lowest transverse mode and does not change this mode. Therefore the problem can be transformed to a 1D transmission problem. However, the confinement potential is not sufficient to cause a rectification. The main reason for the rectification is the change in the charge density of the electrons around the scatterer in an asymmetric manner.

REFERENCES

[1] Datta, S. *Electronic Transport in Mesoscopic Systems*. Cambridge University Press, (1995).

[2] Linke, H., Humphrey, T. E., Lindelof, P. E., Löfgren, A., Newbury, R., Omling, P., Sushkov, A. O., Taylor, R. P., and Xu, H. *Applied Physics A* **75**, 237–246 (2002).

[3] Reimann, P. *Physics Reports* **361**, 57–265 (2002).

[4] Feynman, R. P. *The Feynman lectures on physics*. Reading, Mass., Addison-Wesley Pub. Co., (1963-1964).

[5] Christensson, L., Linke, H., Omling, P., Lindelof, P., Berggren, K., and Zozoulenko, I. *Physical Review B* **57**, 12306 (1998).

[6] Landauer, R. *Philos. Mag.* **21**, 863 (1970).

[7] Büttiker, M., Imry, Y., Landauer, R., and Pinhas, S. *Physical Review B* **31**, 6207 (1985).

[8] van Wees, B. J., van Houten, H., Beenakker, C. W. J., Williamson, J. G., Kouwenhoven, L. P., van der Marel, D., and Foxon, C. T. *Phys. Rev. Lett.* **60**, 848 (1988).

[9] Wharam, D., Thornton, T. J., Newbury, R., Pepper, M., Ahmed, H., Frost, J. E. F., Hasko, D. G., Peacock, D. C., Ritchie, D. A., and Jones, G. A. C. *J. Phys. C: Solid State Phys.* **21**, L209 (1988).

[10] Linke, H., Christensson, L., Omling, P., and Lindelof, P. *Physical Review B* **56**, 1440 (1997).

[11] Linke, H., Sheng, W., Stevensson, A., Löfgren, A., Christensson, L., Xu, H., and Omling, P. *Physical Review B* **61**, 15914 (2000).

[12] Linke, H., Humphrey, T. E., Löfgren, A., Sushkov, A. O., Newbury, R., Taylor, R. P., and Omling, P. *Science* **286**, 2314 (1999).

[13] Xu, H. *Physical Review B* **47**, 15630 (1993).